REPUBLIQUE ALGERIENNE DEMOCRATIQUE ET POPULAIRE
MINISTERE DE L'ENSEIGNEMENT SUPERIEUR ET DE LA RECHERCHE SCIENTIFIQUE
UNIVERSITE MOHAMED BOUDIAF - M'SILA

FACULTE DES SCIENCES
DEPARTEMENT DE PHYSIQUE

N° : Ph/ENR/17/2020

DOMAINE : Sciences de la matière
FILIERE : Physique
OPTION : Physique Energétique et Energies Renouvelables

Mémoire présenté pour l'obtention
Du diplôme de Master Académique

Réalisé par:

Benzitouni Selma

Intitulé

Numerical Simulation of Heat Transfer in a Cylindrical Heat Pipe

Soutenu le 22 / 06 / 2020 devant le jury composé de:

Dr. Baadji Nadjib	Université Mohamed Boudiaf- M'sila	Président
Dr. Boulechfar Hichem	Université Mohamed Boudiaf- M'sila	Rapporteur
Dr. Tayebi Tahar	Université El Bachir El Ibrahimi-BBA	Examinateur

Année universitaire : 2019/2020

To my parents for their endless love, support and encouragement

To my tolerant family

To all my friends

ACKNOWLEDGEMENTS

I thank God Almighty for his abundant grace and blessings bestowed upon me to reach this milestone in my life.

It is a great pleasure for me to put on record my deep sense of gratitude to my supervisor **Dr. Hichem Boulechfar** for his efforts and commitment without forgetting his constant encouragement, his advices and his critics that allowed me to present this modest work.

I would like to thank **Dr. Nadjib Baadji** lecturer at the University of Mohamed Boudiaf, M'sila who gave me the honor to be the president of the jury for my master thesis.

My sincerely appreciation is extended to **Dr. Tahar Tayebi** lecturer at the University of El Bachir El Ibrahimi, Bordj Bou Arreridj who agreed to be part of the jury despite the difficult circumstances.

TABLE OF CONTENTS

LIST OF FIGURES

NOMENCLATURE

Roman letters:

R_o	External cylinder radius	[m]
R_i	Internal cylinder radius	[m]
T_0	Reference temperature	[K]
T_1	Internal wall temperature	[K]
T_2	External wall temperature	[K]
T_{cold}	Cold temperature $T_{cold} = T_2$	[K]
T_{hot}	Hot temperature $T_{hot} = T_1$	[K]
t	Time variable	[s]
g	Gravitational acceleration	[m/s^2]
U_R	Velocity component in (r)direction	[m/s]
U_θ	Velocity component in (θ)direction	[m/s]
U_z	Velocity component in (z)direction	[m/s]
P	Pressure	[Pa]
C_p	Specific heat capacity	[$J.kg^{-1}.k^{-1}$]
r	Radial Coordinate	[m]
r*	Dimensionless radial coordinate $\frac{r}{R_i}$	
U_r^*	Dimensionless Velocity component in (r)direction $\frac{U_r}{\alpha/R_i}$	
U_θ^*	Dimensionless Velocity component in (θ)direction $\frac{U_\theta}{\alpha/R_i}$	
T*	Dimensionless temperature $\frac{T-T_2}{T_1-T_2}$	
P*	Dimensionless pressure $\frac{P}{\rho(\frac{\alpha}{R_i})^2}$	
A	Aspect ratio $\frac{R_0}{R_i}$	
Pr	Prandtl number $\frac{\nu}{\alpha}$	
Ra	Rayleigh number $\frac{g\,\beta\,\Delta T\,R_i^3}{\nu\,\alpha}$	
K	Porous medium permeability	[m^2]
$\vec{U}$	Darcy velocity vector	[m/s]

Greek letters

β_T	Coefficient of thermal expansion	[1/K]
ρ	Density of the fluid	[kg/m^3]
ρ_0	Density at the reference temperature	[kg/m^3]
λ	Thermal conductivity	[w/m. k]
α	Thermal diffusivity	[m^2/s]
μ	Dynamic viscosity	[kg. m^{-1}.s^{-1}]
υ	Kinematic viscosity	[m^2/s]
θ	The azimuth angle	[rad]

Subscripts

1	Internal
2	External
o	Outer
i	Inner
r, θ,z	Cylindrical coordinate

Superscript

*	Dimensionless.

INTRODUCTION

One of the major challenges for the time being, in many fields and applications is reducing energy consumption as well as the energy control. Over the last years, the worldwide energy consumption has been rapidly increased, and the energy supply has become one of the important concerns of every government in the world. The deteriorating economy have fully reflected the scarcity of the conventional energy resources and the wide gap between rising demand and limited supply in the energy market as that resources are nonrenewable and being consumed far faster than being replaced. Moreover, their gaseous emissions lead to a many environmental problems like global warming and ozone depletion. Therefore, the heat management solutions have become more required nowadays and have recommended for more energy conservation efficient devices such as heat exchanger and heat pipe that are extremely used in the energy storage and recovery system.

The heat pipe technology is already successfully implemented in varied industrial thermal management applications like electronic cooling, spacecraft thermal control, transportation systems, solar systems and automotive industry. It also had a very important role in the heat exchangers function improvements and energy saving and show that it could manage a wide range of industrial applications with the indisputable advantage of being cheaper and more flexible in different shapes and designs. However, the internal modeling of the physics that govern this device operation presents a challenging problem for the engineers and researchers to study its thermal performance which is greatly affected by several parameters such as geometry, dimensions, working fluid, wick materials etc.

For that purpose, the numerical resolution has become an important and useful method for this kind of complex studies. In the presented work we proposed a numerical simulation of heat transfer within a cylindrical heat pipe using COMSOL Multiphysics package which is based on the finite element method. The mathematical model is described by Navier stokes and energy equations and constitutive porous medium flow model to predict the behavior of the flow in the heat pipe cross section using some necessary assumptions to simplify the problem.

The objective of this work is to determine the effect of different parameters such as Rayleigh number, permeability and aspect ratio on the flow structure, temperature distribution and velocity field within the annular space that represents a heat pipe cross section for two cases. The first one where the annular space is filled with Newtonian fluid (air) and the second one with a fluid saturated porous medium.

The manuscript consists of four chapters. In the first chapter we provided an overview on heat transfer, the basics of heat pipes and previous works available in the literature that performed a various studies on heat pipe, the second chapter describes the mathematical model that have used in this work, including details on heat pipe structure, the governing equations in cylindrical coordinates, their dimensionless form and the boundary conditions and assumptions. In The third chapter we exposed an overview on Comsol Multiphysics software and the numerical simulation steps to solve the equations that describe the problem.

The fourth and the last chapter which is devoted to the results and their discussions, is divided into two parts after validation process , the first part of the results deals with the case where the annular space is filled with air, while the second part deals with the space filled with fluid saturated porous medium. We completed the manuscript with a conclusion that summarizes the main results.

CHAPTER I:
GENERAL INFORMATION AND LITERATURE REVIEW

1.1 Overview on heat transfer :

Heat can be transferred from one body to another or from one location in a same body to another and this process is known as heat Transfer which is the science that seeks to predict the energy transferred between bodies as a result of a temperature difference. Heat only flows from a body at higher temperature to another at lower temperature. Although this look obvious, but this natural law is very important from the thermodynamics point of view. The science of heat transfer seeks not merely to explain how heat is transferred, but also to predict the rate at which the exchange will take place under certain specified conditions. **[1]**

Three mechanisms of heat transfer are important in the environment of plants and animals: radiation, convection which is the transfer of heat by moving air or fluid, and conduction in solids (and non-moving gases and fluids) which depends on the exchange of kinetic energy between molecules. Two types of convection are important, forced convection and free convection which a result of density difference. **[2]**

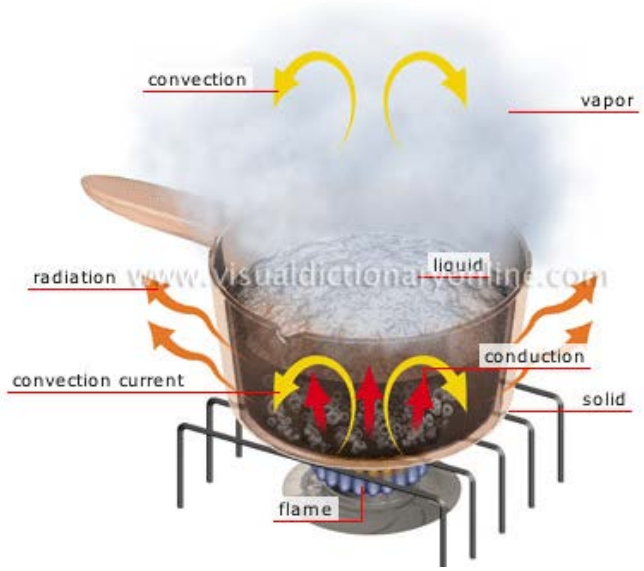

Figure 1.1: Modes of heat transfer**. [3]**

1.2 Background on heat pipe :

The heat pipe is one of the remarkable achievements of thermal physics and heat transfer engineering in this century because of its unique ability to transfer heat over large distances

without considerable losses **[4].** Generally, it is a heat mover or heat spreading device and it acquires heat from a source and transfers or spreads it to a sink region. The heat transfer ability is the most important factor, and it has to be designed to maximize with various influencing parameters. It needs very little drop in temperature to move the heat. Typically the heat pipe is a simply sealed and vacuumed tube with a porous wick structure to generate capillary force which is the most important factor to improve the heat transfer performance and a very small amount of working fluid is charged inside.

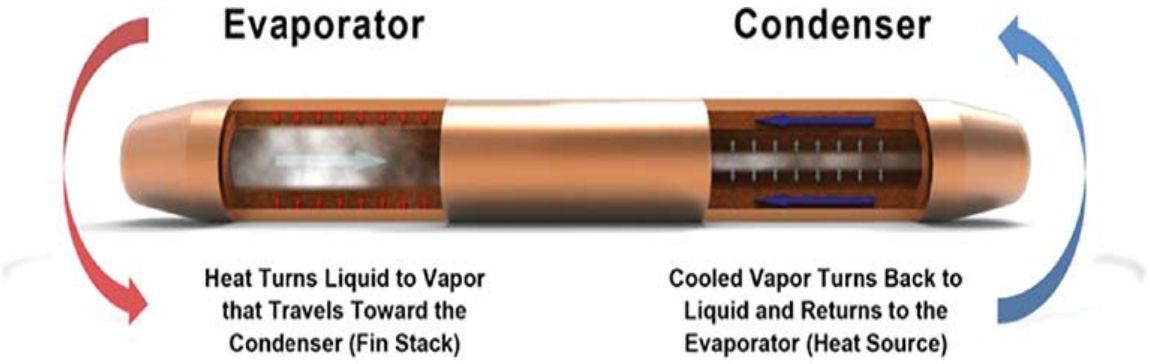

Figure 1.2: Cylindrical heat pipe **[5]**

Various parameters to maximize heat transfer ability of a heat pipe are influenced by working fluids such as nanofluids, pumping pressure, friction loss toward length, charging ratio, inclination angle, and so on. **[6-7]** If there is no structural change in the heat pipe such as porous wick, container, orientation, diameter, length and other changes, the working fluid is the main solution to improve the heat transfer performance of heat pipe. The correct choice of working fluid is the important factor which can lead to decrease the thermal resistance of a heat pipe. In recent days, nanofluids as the new working fluids of heat pipe have been tried to be adopted as the heat transfer fluid. **[8-9]**

Due to their low weight, zero maintenance, low cost and reliable functionality, heat pipe applications are varied from aerospace engineering to consumer specific electronic devices such as power supplies, laptop and desktop computers, audio amplifier components… etc. From the electronics cooling and HVAC applications to biomedical engineering, all these applications are

because of its great design flexibility, high thermal effectiveness, simple fabrication, and easy control.

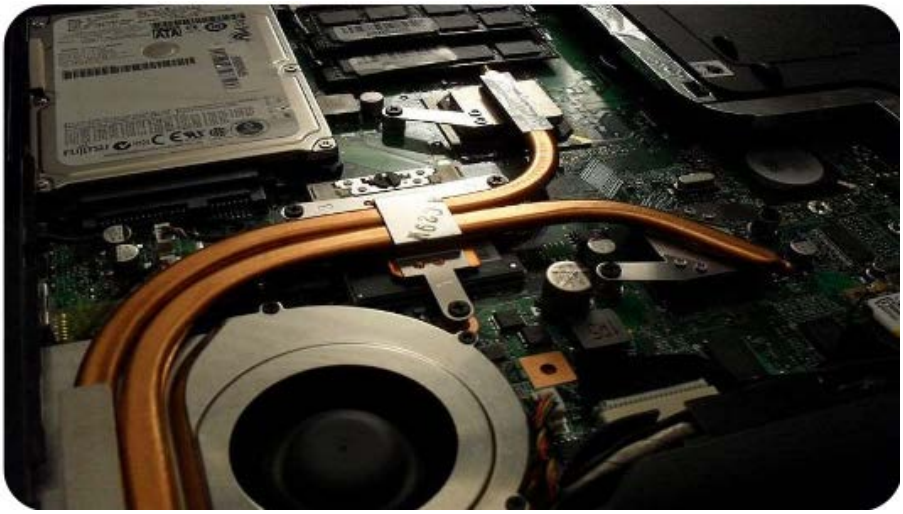

Figure 1.3: Laptop computer heat pipe system **[10]**

Many different types of heat pipes As micro heat pipe , pulsating heat pipe and loop heat pipe and other types developed in recent years to address electronics thermal management problems **[11,12]** , solar energy **[13,14]** as well as lots of other applications [**12,15,16]** and are shown promising results. Some of these types are illustrated as follows:

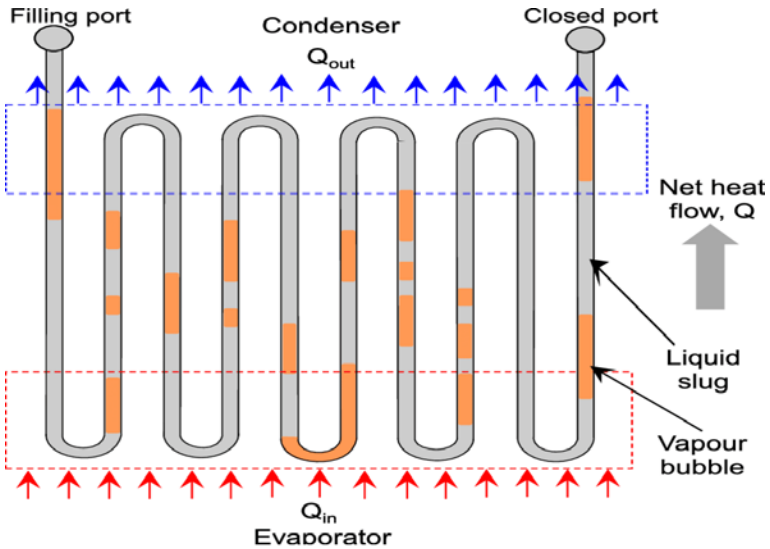

Figure 1.4 Schematic of an oscillating heat pipe **[17]**

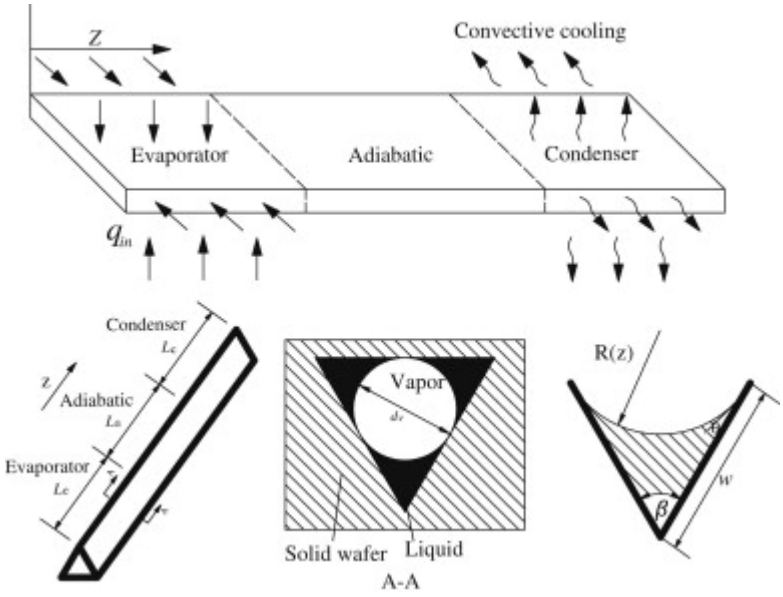

Figure 1.5: Geometry of micro-heat pipe **[18]**

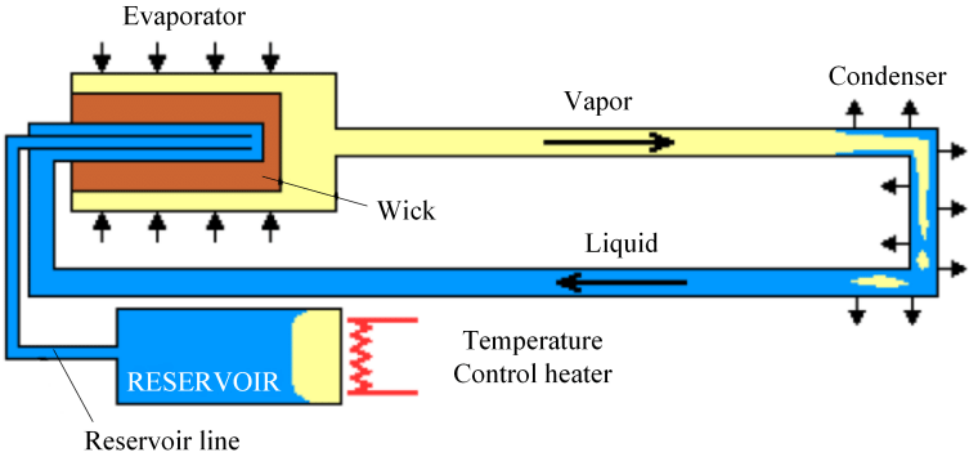

Figure 1.6: Geometry of loop heat pipe **[19]**

1.3 Fundamentals of Heat Pipe:

Heat pipes are passive heat transfer devices, which have very long lives when properly designed and fabricated. Long life is critical in applications such as spacecraft thermal control, where heat pipes in satellites can operate for decades, with no opportunity for repair or replacement. Most of the problems with long term operation of heat pipes are caused by material compatibility between the working fluid and the heat pipe material **[20]** The operations of a heat pipe are simply explained based on a cylindrical geometry as an example, shown in Figure (1.8). However, the shape and size of the heat pipes can be different as we mentioned previously.

Heat pipes are consisted of a closed container or envelope (pipe wall and end caps), a wick structure, and working liquid in equilibrium state with its own vapor. Most used working fluid choices are water, acetone, methanol, ammonia, or sodium depending on the operating temperature. The external walls of heat pipe are split into three sections: the evaporator section, adiabatic section and condenser section. Although, a heat pipe can have no adiabatic section and also could have multiple evaporation and condensation sections depending on specific applications and design.

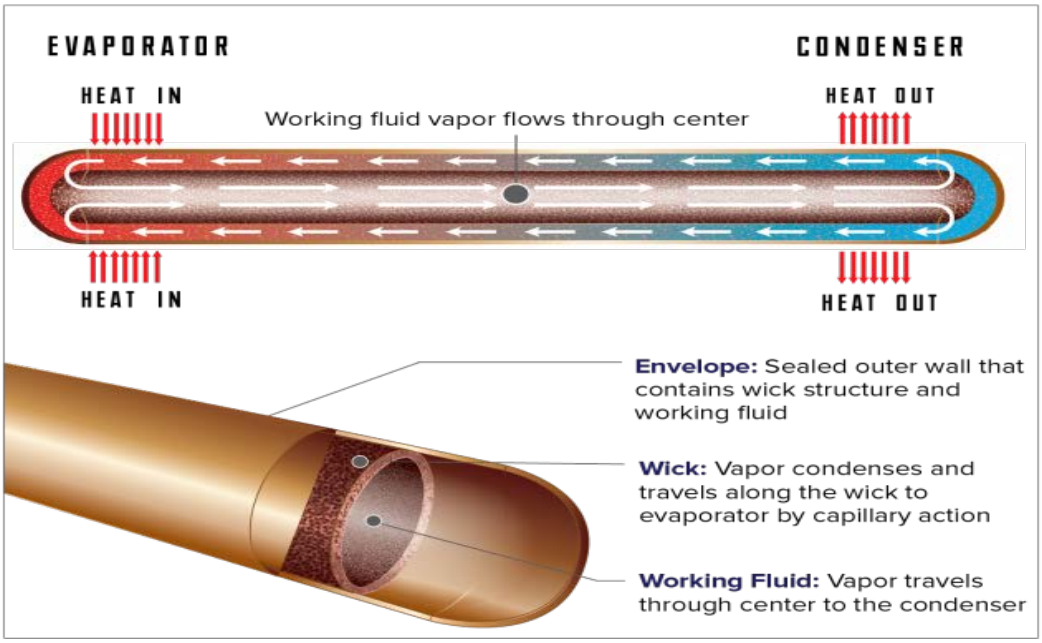

Figure 1.7: Heat pipe components **[21]**

The heat input vaporizes the working fluid in liquid form at the wick surface in the evaporator section. Vapor and its associated latent heat flow toward the colder condenser section, where it condenses, giving up the latent heat. Capillary action then moves the condensed liquid back to the evaporator through the wick structure.

Essentially, this operates in the same way as how a sponge soaks up water. Phase-change processes and the two-phase flow circulation in the heat pipe will continue as long as there is a large enough temperature difference between the evaporator and condenser sections. The fluid stops moving if the overall temperature is uniform, but starts back up again as soon as a temperature difference exists. No power source (other than heat) is needed. In some cases, when the heated section is below the cooled section, gravity is used to return the liquid to the evaporator. However, a wick is required when the evaporator is above the condenser on earth. A wick is also used for liquid return if there is no gravity, such as in NASA's micro-gravity applications **[21]**

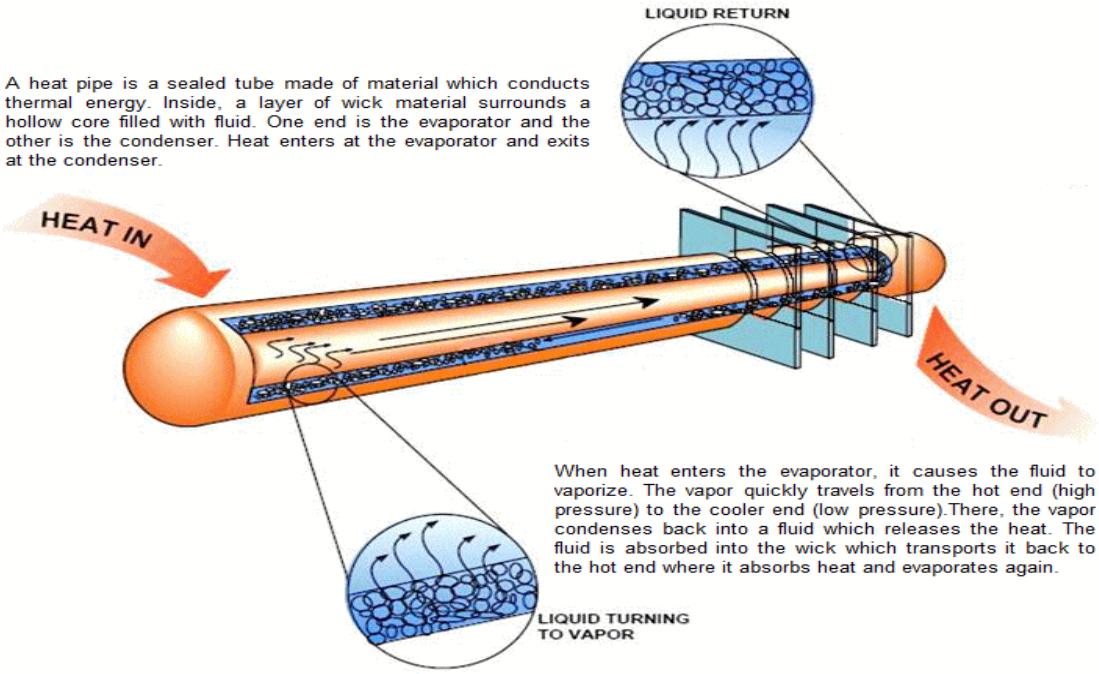

Figure 1.8: Heat pipe operations **[22]**

Basically, heat pipe theory deals with fundamentals of hydrodynamic and heat transfer and combines the principles of both thermal conductivity as well convection and conduction in solid

and fluid domains and phase transition to efficiently manage the transfer of heat between two solid interfaces.

1.4 Literature Review:

There are many analytical and numerical studies on heat pipe based on varieties of assumptions and problems. One of those studies in heat pipes was published by **[23] Eui Guk Jung and Joon Hong Boo** studied the steady-state analytical modeling of a loop heat pipe (LHP) equipped with a flat evaporator was presented to predict the temperatures and pressures at each important part of the LHP evaporator. **[24] E.Mezaache, A.Omara and M.S.Ferah** elaborated also a one dimensional model to study the heat and mass transfer in a stationary variable conductance heat pipe with uniform pressure, this model can be considered as an extension of **[25] Sun's and Tien's** model to take account for vapor-gas diffusion. [**26] Boulahrouz Salim** presented a numerical simulation of the thermohydraulic behavior of a two phase loop thermo-syphon used for cooling of power electronic components, the model supposed that the vapor flow is monodimensional and permanent and the finite volumes method was used for the discretisation of the model equations. **[27] Hamidreza Behi** investigated experimentally and numerically the thermal performance, energy storage and cooling capacity of a heat pipe assisted Phase Change Material (PCM) storage system in order to study the effect of using heat pipe on energy storage system performance and miniature cooling applications**. [28] Vikas Kumard, Gangacharyulu and Ram Gopal Tathgir** reported a theoretical and experimental study of a wire screen heat pipe computed thermal resistances at the external surface of the evaporator and condenser as well as inside the heat pipe, the theoretical study deals with the development of an analytical model based on thermal resistance network approach. **[29] Nicolas Blet, Stéphane Lips, Valérie Sartre** presented a summary of heat pipe was described for the function of temperature homogenization then performed and identified their specificities, compared to other applications of heat pipes. **[30] Cheayb Mohamad** provided a hydrodynamic modeling of the thermal behaviors of flat miniature heat pipes, geometry configuration and the design of the fin array that enhances heat transfer by natural convection which allowed developing a passive cooling solution. **[31] Lora Kamenova** employed a thermo-hydraulic modeling of miniature heat pipes thin plates to study the performances of flat heat pipes with sintered powder capillary wick, reported as thermal functions in high density electronics. **[32] Mehdi Famouri** introduced a

robust numerical scheme employed and developed to investigate transient and steady-state operation of cylindrical heat pipes with hybrid wick structure for high heat fluxes based on an incompressible flow model. **[33] Mohamed noorul hussain and Isam janajreh** studied a numerical simulation method to analyze the performance of the heat pipe depended on four parameters namely, porosity, condenser evaporator lengths and radius of the heat pipe and the heat input, in terms of the absolute thermal resistance.

CHAPTER II:
MODEL DESCRIPTION

2.1 Introduction:

In this chapter, we formulate the physical problem mathematically based on a cylindrical heat pipe where different mechanisms of heat transfer are involved. Because of the coupled phenomena that occur during the heat pipe working process we have retained some assumptions therefore to simplify our problem and to apply the fundamental physical laws to obtain the mathematical model which describe the physical problem.

2.2 Problem description:

In the present analysis, basically heat is applied at the evaporator section causes vaporization and subsequent pressurization of the working liquid. The vapor flows to the condenser section and releases latent heat as it condenses. The heat is then removed from the condenser wall surface by convection as is shown in figure (2.1). The physical domain shown in figure (2.2) in our case represents a cross section of the heat pipe with reference to the radius of the outer and the inner cylinders R_i, R_o. We consider a cylindrical coordinate system with z-axis along the axial direction of the heat pipe cylinder and the radial direction r perpendicular to z-axis and the azimuth angle θ. In our two dimensional case the geometry is represented in the polar coordinates system. The heat pipe cross section represents an annulus space filled with porous medium known as wick structure. In the context of the current work, transfer of thermal energy in the solid matrix and the fluid phase takes place by means of two different processes. Firstly, by means of conduction process that involves the transfer of thermal energy through the solid matrix of the porous medium. Secondly, by means of free convection involving the transfer of thermal energy in the annular space that contains a porous medium saturated with the working fluid (air).

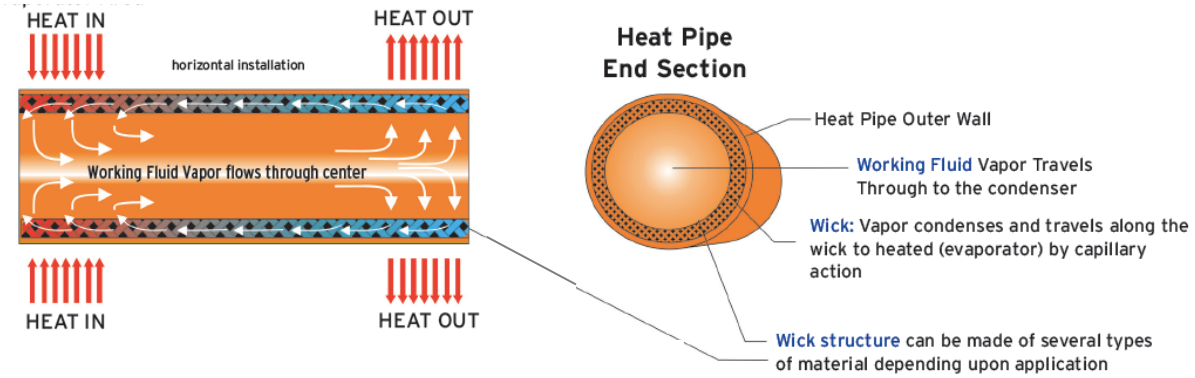

Figure 2.1: Heat pipe tube representation **[34]**

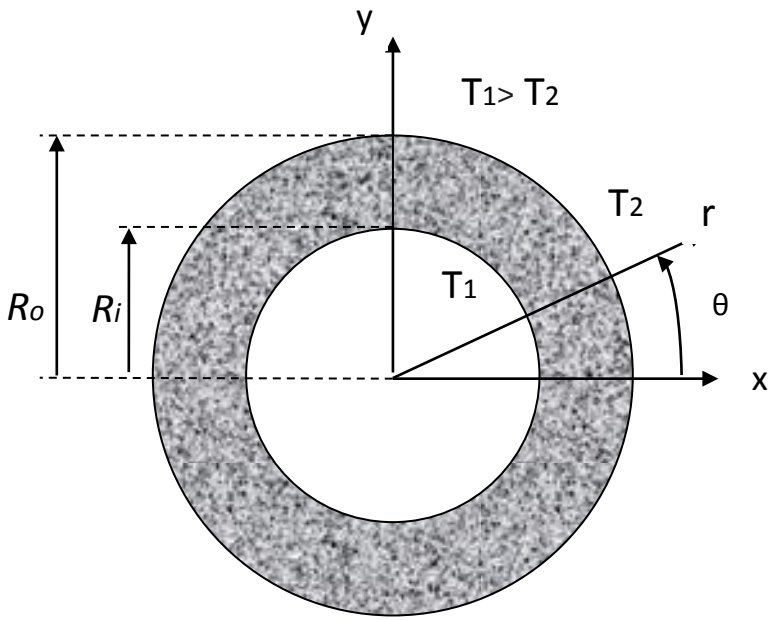

Figure 2.2: Heat pipe cross section

2.3 Assumptions

- The flow is assumed to be bidimensional, steady, laminar.
- The working fluid is presumed to be Newtonian and incompressible.
- It is assumed that the effect of the shell thickness is neglected
- The porous medium is considered homogeneous and isotropic.
- It is assumed that no condensation occurs in the study domain.
- It is assumed that there is no heat generation source inside the heat pipe.
- Viscous dissipation in the energy equation is neglected.
- The Boussinesq approximation is used for the variations of the density in the terms of force of volume when they give rise to gravitational force.
- The physical properties of the fluid are constant in the other terms in the equations.

Therefore the fluid density change can be described based on the reference temperature T_0 as follows:

$$\rho = \rho_0(1 - \beta_T(T - T_0)) \quad (2.1)$$

$\beta_T = -\frac{1}{\rho_0}\frac{\partial \rho}{\partial T}$: The coefficient of thermal expansion

2.4 Governing Equations:

The general governing equations expressed in the cylindrical coordinates (r, θ, z) are given as following:

- **Continuity equation :**

$$\rho\left(\frac{\partial \vec{\rho}}{\partial t} + \overrightarrow{\nabla}.\overrightarrow{V}\right) = 0 \quad (2.2)$$

$$\rho\left(\frac{\partial \rho}{\partial t} + \frac{\partial U_r}{\partial r} + \frac{U_r}{r} + \frac{1}{r}\frac{\partial U_\theta}{\partial \theta} + \frac{\partial U_z}{\partial z}\right) = 0 \quad (2.3)$$

- **Momentum equation :**

$$\rho\left(\frac{\partial \vec{U}}{\partial t} + \vec{U}.\vec{\nabla}\, U\right) = -\nabla P + \rho\vec{g} + \mu\nabla^2 U \quad (2.4)$$

- In (r-direction):

$$\rho\left(\frac{\partial U_r}{\partial t} + U_r\frac{\partial U_r}{\partial r} + \frac{U_\theta}{r}\frac{\partial U_r}{\partial \theta} + U_z\frac{\partial U_r}{\partial z} - \frac{U_\theta^2}{r}\right) = -\frac{\partial P}{\partial r} + \mu\left(\frac{\partial^2 U_r}{\partial r^2} + \frac{1}{r}\frac{\partial U_r}{\partial r} + \frac{1}{r^2}\frac{\partial^2 U_r}{\partial \theta^2} + \frac{\partial^2 U_r}{\partial z^2} - \frac{U_r}{r^2} - \frac{2}{r}\frac{\partial U_\theta}{\partial \theta}\right) + \rho g_r \quad (2.5)$$

- In (θ- direction):

$$\rho\left(\frac{\partial U_\theta}{\partial t} + U_r\frac{\partial U_\theta}{\partial r} + \frac{U_\theta}{r}\frac{\partial U_\theta}{\partial \theta} + U_z\frac{\partial U_\theta}{\partial z} - \frac{U_r U_\theta}{r}\right) = -\frac{1}{r}\frac{\partial P}{\partial r} + +\mu\left(\frac{\partial^2 U_\theta}{\partial r^2} + \frac{1}{r}\frac{\partial U_\theta}{\partial r} - \frac{1}{r^2}\frac{\partial^2 U_\theta}{\partial \theta^2} + \frac{\partial^2 U_\theta}{\partial z^2} - \frac{U_\theta}{r^2} + \frac{2}{r^2}\frac{U_r}{\partial \theta}\right) + \rho g_\theta \quad (2.6)$$

- In(z -direction)

$$\rho\left(\frac{\partial U_z}{\partial t} + U_r\frac{\partial U_z}{\partial r} + \frac{U_\theta}{r}\frac{\partial U_z}{\partial \theta} + U_z\frac{\partial U_z}{\partial z}\right) = -\frac{\partial P}{\partial z} + \mu\left(\frac{\partial^2 U_z}{\partial r^2} + \frac{1}{r}\frac{\partial U_z}{\partial r} + \frac{1}{r^2}\frac{\partial^2 U_z}{\partial \theta^2} + \frac{\partial^2 U_z}{\partial z^2}\right) + \rho g_z \quad (2.7)$$

- **The energy equation:**

$$\rho\left(\frac{\partial T}{\partial t} + \vec{U}.\vec{\nabla}T\right) = \frac{\lambda}{C_p}(\nabla^2 T) \quad (2.8)$$

$$\rho\left(\frac{\partial T}{\partial t}+U_r\frac{\partial T}{\partial r}+\frac{U_\theta}{r}\frac{\partial T}{\partial \theta}+U_z\frac{\partial T}{\partial z}\right)=\frac{\lambda}{C_p}\left(\frac{\partial^2 T}{\partial r^2}+\frac{1}{r}\frac{\partial T}{\partial r}+\frac{1}{r^2}\frac{\partial^2 T}{\partial \theta^2}+\frac{\partial^2 T}{\partial z^2}\right) \quad (2.9)$$

Under the assumptions that we mentioned previously, the equations of continuity, momentum and energy balance are rewritten as follows:

- **The continuity equation:**

$$\frac{\partial U_r}{\partial r}+\frac{U_r}{r}+\frac{1}{r}\frac{\partial U_\theta}{\partial \theta}=0 \quad (2.10)$$

- **The Momentum equation**:

$$\rho\left(U_r\frac{\partial U_r}{\partial r}+\frac{U_\theta}{r}\frac{\partial U_r}{\partial \theta}-\frac{U_\theta^2}{r}\right)=-\frac{\partial P}{\partial r}+\mu\left(\frac{\partial^2 U_r}{\partial r^2}+\frac{1}{r}\frac{\partial U_r}{\partial r}+\frac{1}{r^2}\frac{\partial^2 U_r}{\partial \theta^2}-\frac{U_r}{r^2}-\frac{2}{r^2}\frac{\partial U_\theta}{\partial \theta}\right)$$

$$+g\rho\cos\theta\,\beta(T-T_0) \quad (2.11)$$

$$\rho\left(U_r\frac{\partial U_\theta}{\partial r}+\frac{U_\theta}{r}\frac{\partial U_\theta}{\partial \theta}-\frac{U_rU_\theta}{r}\right)=-\frac{1}{r}\frac{\partial P}{\partial r}+\mu\left(\frac{\partial^2 U_\theta}{\partial r^2}+\frac{1}{r}\frac{\partial U_\theta}{\partial r}+\frac{1}{r^2}\frac{\partial^2 U_\theta}{\partial \theta^2}-\frac{U_\theta}{r^2}+\frac{2}{r^2}\frac{\partial U_r}{\partial \theta}\right)$$

$$+g\rho\sin\theta\,\beta(T-T_0) \quad (2.12)$$

- **The energy equation:**

$$\rho\left(U_r\frac{\partial T}{\partial r}+\frac{U_\theta}{r}\frac{\partial T}{\partial \theta}\right)=\frac{\lambda}{C_p}\left(\frac{\partial^2 T}{\partial r^2}+\frac{1}{r}\frac{\partial T}{\partial r}+\frac{1}{r^2}\frac{\partial^2 T}{\partial \theta^2}\right) \quad (2.13)$$

$\alpha=\frac{\lambda}{\rho C_p}$: The thermal diffusivity

2.5 The boundary conditions:

The resolution of the equations system requires the incorporation of the boundary conditions for each dependent variable. The boundary conditions that apply to this problem are listed below:

- The internal wall: r =R_i

$U_r = U_\theta = 0$

$T = T_1 = T_{HOT}$

- The external wall: r =R_o

$U_r = U_\theta = 0$

$T = T_2 = T_{COLD}$

2.6 The dimensionless form of the equations:

In order to control, measure and to reveal the controlling parameters it's recommended to obtain the dimensionless form of the modeling equations that we define based on the following characteristic quantities:

$A = \frac{R_0}{R_i}$: Aspect ratio

$U_r^* = \frac{U_r}{\alpha / R_i}$, $U_\theta^* = \frac{U_\theta}{\alpha / R_i}$

$r^* = \frac{r}{R_i}$

$P^* = \frac{P}{\rho(\frac{\alpha}{R_i})^2}$, $T^* = \frac{(T - T_2)}{(T_1 - T_2)}$

Continuity equation:

$$\frac{\partial U_r^*}{\partial r^*} + \frac{U_r^*}{r^*} + \frac{1}{r^*}\frac{\partial U_\theta^*}{\partial \theta} = 0 \qquad (2.14)$$

- Momentum equation:

- In (r-direction):

$$\left(U_r^* \frac{\partial U_r^*}{\partial r^*} + \frac{U_\theta^*}{r^*}\frac{\partial U_r^*}{\partial \theta} - \frac{U_\theta^{*2}}{r^*}\right) = -\frac{\partial P^*}{\partial r^*} + Pr\left(\frac{\partial^2 U_r^*}{\partial r^{*2}} + \frac{1}{r}\frac{\partial U_r^*}{\partial r^*} + \frac{1}{r^{*2}}\frac{\partial^2 U_r^*}{\partial \theta^2} - \frac{U_r^*}{r^2} - \frac{2}{r^{*2}}\frac{\partial U_\theta^*}{\partial \theta}\right) + Pr.Ra.\cos\theta\, T^* \qquad (2.15)$$

- In (θ- direction):

$$\left(U_r^* \frac{\partial U_\theta^*}{\partial r^*} + \frac{U_\theta^*}{r^*}\frac{\partial U_\theta^*}{\partial \theta} - \frac{U_r^* U_\theta^*}{r}\right) = -\frac{1}{r^*}\frac{\partial P^*}{\partial \theta^*} + Pr\left(\frac{\partial^2 U_\theta^*}{\partial r^{*2}} + \frac{1}{r}\frac{\partial U_\theta^*}{\partial r^*} + \frac{1}{r^{*2}}\frac{\partial^2 U_\theta^*}{\partial \theta^2} - \frac{U_\theta^*}{r^{*2}} + \frac{2}{r^{*2}}\frac{U_r^*}{\partial \theta}\right) + Pr.Ra.\sin\theta\, T^* \quad (2.16)$$

Energy equation:

$$\left(U_r^* \frac{\partial T^*}{\partial r^*} + \frac{U_\theta^*}{r^*}\frac{\partial T^*}{\partial \theta}\right) = \left(\frac{\partial^2 T^*}{\partial r^{*2}} + \frac{1}{r^*}\frac{\partial T^*}{\partial r^*} + \frac{1}{r^{*2}}\frac{\partial^2 T^*}{\partial \theta^2}\right) \quad (2.17)$$

Where:

$\Pr = \frac{v}{\alpha} = \frac{\mu C_P}{\lambda}$ Prandtl number

$Ra = \frac{g\beta \Delta T R_i^3}{v\alpha}$ Rayleigh number

2.7 Porous medium constitutive model:

Several momentum flow models have been proposed to model the fluid flow through a porous media. The aim was to develop a macroscopic equation which matches the empirical observations and which converges to the corresponding free fluid flow when the porosity of the porous media tends towards unity problems of momentum transport in porous media arise from the fact that mismodeling of the velocity distribution will strongly affect the temperature distribution. Therefore, there is a need to focus on these momentum models before considering any model describing the temperature distribution. The first momentum equation which describes the transport phenomenon of the fluid flow through porous media was deduced experimentally in 1856 by Henry Darcy. Darcy's law represents the resistance which is the friction offered by the solid particles to the fluid flow **[35]**. According to this law the fluid flow is linearly dependent upon the pressure gradient and the gravitational force with proportionality factor is generally known as the permeability. Since the development of Darcy flow model several attempts have been made to derive it analytically starting from the Navier-Stokes equation. These derivations show that this flow model is restricted to a flow in which the viscous forces dominate over the inertia forces which means that Darcy's law is only valid for slow viscous flow. However, because the Darcy flow model is of order one less than the Navier-Stokes equation, the no-slip hydrodynamic boundary condition cannot be applied and therefore Brinkman's equation which also known as Brinkman's extension of Darcy's law was developed.

The Brinkman equation describe flow in porous media that is fast enough that the drive for flow includes kinetic potential related to fluid velocity, pressure, and gravitational potential. It appears as a mix of Darcy's law and the Navier-Stokes equations and extends Darcy's law to account for dissipation of kinetic energy by viscous shear as in the Navier-Stokes equation. The Brinkman equation often describe the transition between slow flow in porous media that is governed by Darcy's law and fast flow in channels as it described by the Navier Stokes equations below :

$$-\frac{\mu}{K}\vec{U} = \left(\rho\vec{g} - \vec{\nabla}P\right) + \mu\nabla^2 U \qquad (2.18)$$

Where:

$\vec{U}$: Darcy velocity vector

K: Permeability of porous medium

ρ and μ are respectively the density and the dynamic viscosity of the fluid.

$\vec{g}$: The gravitational force vector

$\vec{\nabla}P$: The pressure gradient

The Brinkman model removes the deficiency of Darcy law in the sense that it is applicable to media with high permeability and can account for all boundary conditions at a solid surface or at a fluid interface.

Chapter III:

NUMERICAL RESOLUTION

3.1 Introduction:

The equations that governed the natural convection in porous medium that we exposed in the previous chapter must be resolved to know the characteristics of this thermal field. But, it is practically impossible to find an exact analytical solution to such system because the equations system is very complex. Therefore, it's recommended to choose an appropriate numerical method to solve the problem. In this chapter we introduce Comsol Multiphysics software as a relevant choice for a numerical simulation to solve our equations system with their associated boundary conditions in order to obtain the best approximations.

3.2 COMSOL software Overview: [36]

Numerical simulation has become essential tool for the design process and it is widely used nowadays for the validation and evaluation of smart grid solutions and applications area as Geophysics, Optics, Porous media flow…etc. Certain types of Computer simulation Software have been introduced for the purpose of analyzing heat transfer efficiently and COMSOL Multiphysics software is one of them. COMSOL Multiphysics is commercial software based on finite element analysis method and a powerful interactive environment for modeling and solving all kinds of scientific and engineering problems based on partial differential equations (PDEs). At the beginning time, this software was only applied in the field of Structural Mechanics, but now with this product we can easily extend conventional models for one type of physics into Multiphysics models that solve coupled physics phenomena.

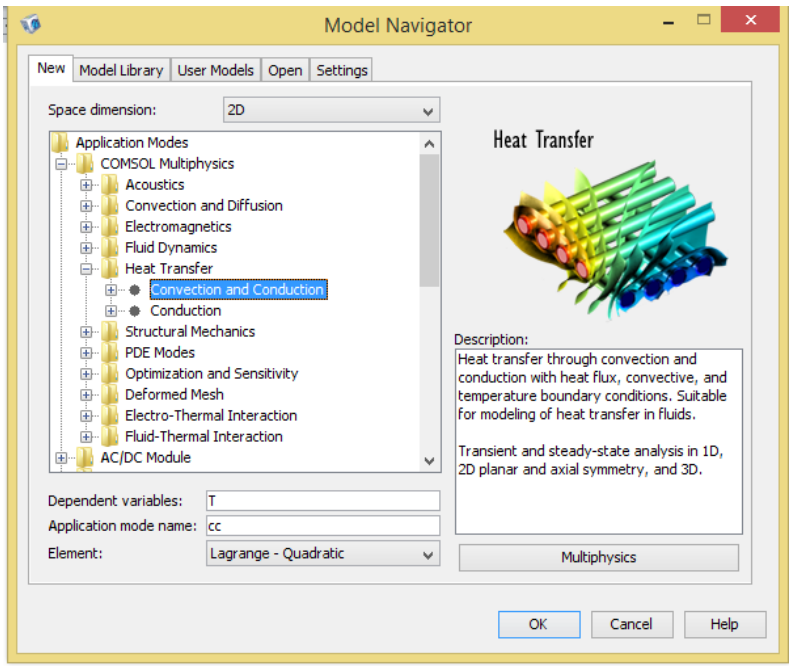

Figure 3.1: The interface of COMSOL Multiphysics software

Accessing this powerful tool does not require an in-depth knowledge of mathematics or numerical analysis. The built-in physics modes allows to build models by defining the relevant physical quantities such as material properties, boundary conditions, sources, and fluxes rather than by defining the underlying equations, COMSOL Multiphysics then internally compiles a set of PDEs representing the entire model.

COMSOL Multiphysics gives two options for the user to access to the software environment, one as a standalone product through a flexible graphical user interface, and the other option is by script programming in the MATLAB language, this gives the freedom to combine PDE based modeling, simulation, and analysis with other modeling techniques.

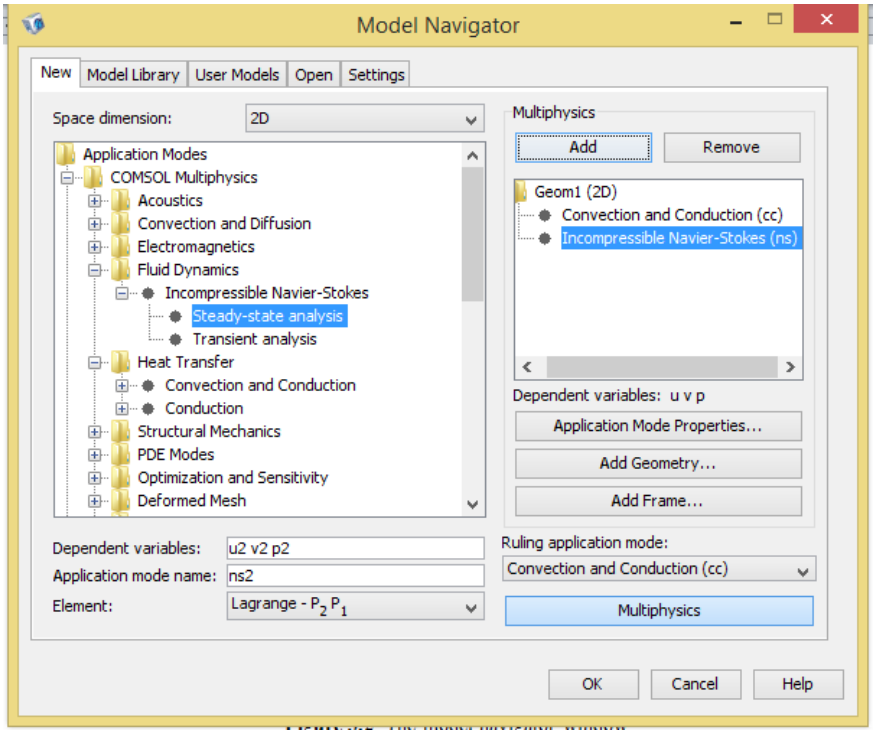

Figure 3.2: Model navigator window

Solving PDEs generally will take time to set up the underlying equations, material properties, and boundary conditions for a given problem, COMSOL Multiphysics reduce huge amount of this work. Another unique feature of this program is the ability to combine domains of different space dimensions in the same problem. This flexibility not only simplifies modeling, it also can decrease execution time.

COMSOL Multiphysics application window provides a graphical user interface (GUI) for 1D, 1D axisymmetric, 2D, 2D axisymmetric, and 3D geometries that handles all aspects of the modeling process.

Using the application modes in COMSOL Multiphysics gives us the possibility to perform various types of analysis including:

• Stationary and time-dependent analysis

• Linear and nonlinear analysis

• Eigenfrequency and modal analysis

To solve the PDEs, COMSOL Multiphysics uses the proven finite element method (FEM). The software runs the finite element analysis together with adaptive meshing and error control using a variety of numerical solvers.

3.3 Finite element method (FEM):

The finite element method (FEM) is a numerical technique for solving problems which are described by partial differential equations or can be formulated as a functional minimization. The approximating functions (interpolation functions) in finite element are defined in terms of the values of the field variables at specified points called nodes or nodal points. Those Nodes usually lay on the element boundaries where adjacent elements are connected. In addition to boundary nodes an element may also have a few interior nodes. Each element is assigned a set of characteristic equations as physical properties, boundary conditions and imposed forces, which are then solved as a set of simultaneous equations to predict the model's behavior.

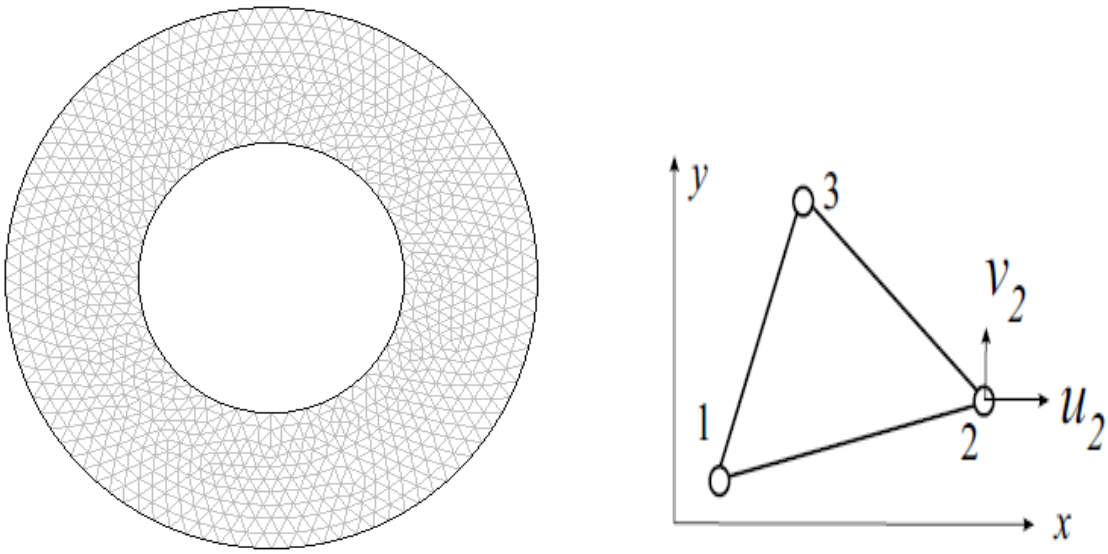

Figure 3.3: Triangular finite element in two dimensions.

Triangular finite element was the first finite element proposed for continuous problems. Because of its simplicity it can be used as an introduction to other element, COMSOL Multiphysics

generally uses finite element in the mathematical sense, where the functions in the finite element space are linear combinations of shape functions.

To summarize in general terms how the finite element method works we list below main steps of the solution procedure:

1) **Discredited the continuum:** The first step is to divide a solution region into finite elements. The finite element mesh is typically generated by a preprocessor program. The description of mesh consists of several arrays main of which are nodal coordinates and element connectivity.
2) **Select interpolation functions:** Interpolation functions are used to interpolate the field variables over the element. Often, polynomials are selected as interpolation functions. The degree of the polynomial depends on the number of nodes assigned to the element.
3) **Find the element properties:** The matrix equation for the finite element should be established which relates the nodal values of the unknown function to other parameters.
4) **Assemble the element equations:** To find the global equation system for the whole solution region we must assemble all the element equations. In other words we must combine local element equations for all elements used for discretization. Element connectivity is used for the assembly process. Before solution, boundary conditions (which are not accounted in element equations) should be imposed.
5) **Solve the global equation system**: The finite element global equation system is typically sparse, symmetric and positive definite. Direct and iterative methods can be used for solution. The nodal values of the sought function are produced as a result of the solution.
6) **Compute additional results**: In many cases we need to calculate additional parameters. For example, in mechanical problems strains and stresses are of interest in addition to displacements, which are obtained after solution of the global equation system.

3.4 Comsol Multiphysics simulation steps:

When creating a model in COMSOL Multiphysics, the typical modeling steps include:

- Application selection
- Creating or importing the geometry
- Meshing the geometry
- Defining the physics on the domains and at the boundaries
- Solving the model
- Postprocessing the solution

- Performing parametric studies

The following section describes the main steps and procedures in COMSOL Multiphysics.

Step 1: Applications module selection:

Here we should selecting the application modes (the principle equations) and specifying variable that we would apply on our geometry from **Multiphysics** menu then **model navigator** button.

The Application modules that we used in this model are shown as model tree:

- Geom1 (2D)
    - Incompressible Navier-Stokes (Earth Science Module)
    - Convection and Conduction in Porous Media (Earth Science Module)

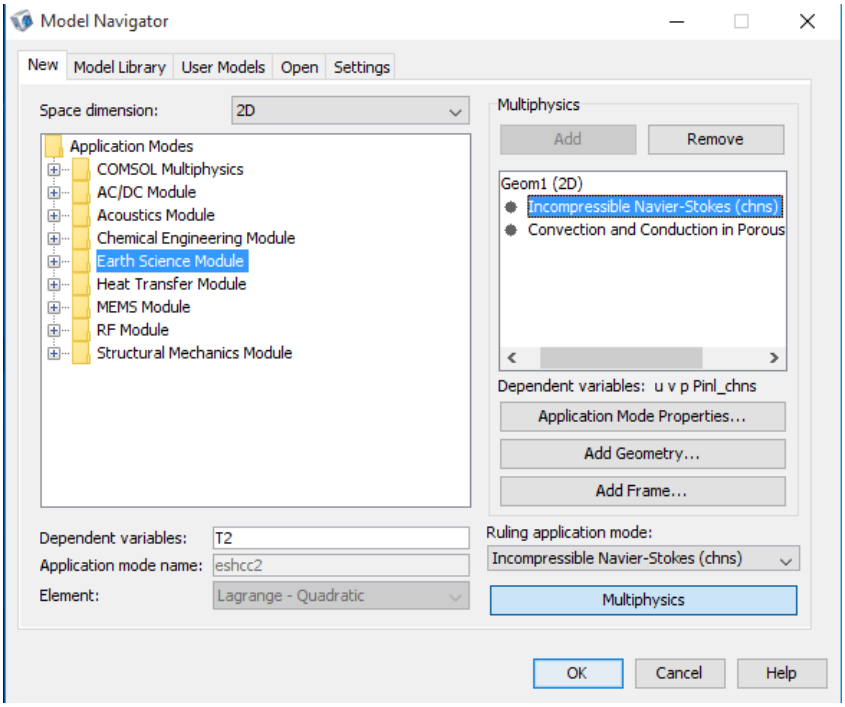

Figure 3.6: Model navigator window

Step 2: Geometry creating

After choosing models and space dimension (2D in our case for example) in the model navigator interface, we begin our simulation work with creating the model geometry using the CAD tools on the draw menu **Draw → specify subject →circle**, and then picking out the subdomain that we would work with from the draw toolbar.

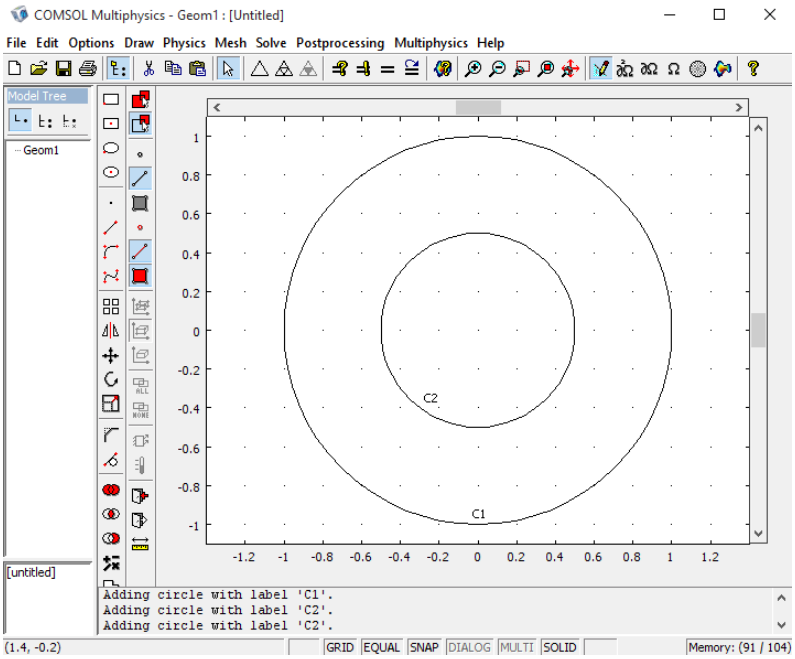

Figure 3.4: Created geometry

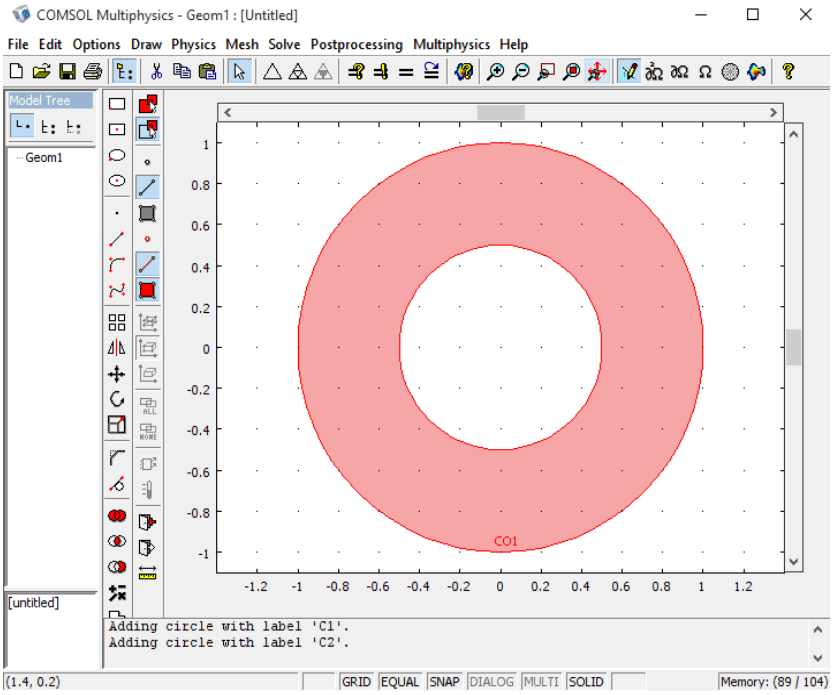

Figure 3.5: The subdomain

Step 3: Options and settings

In this section, we input in the **Options** menu the **constants** list.

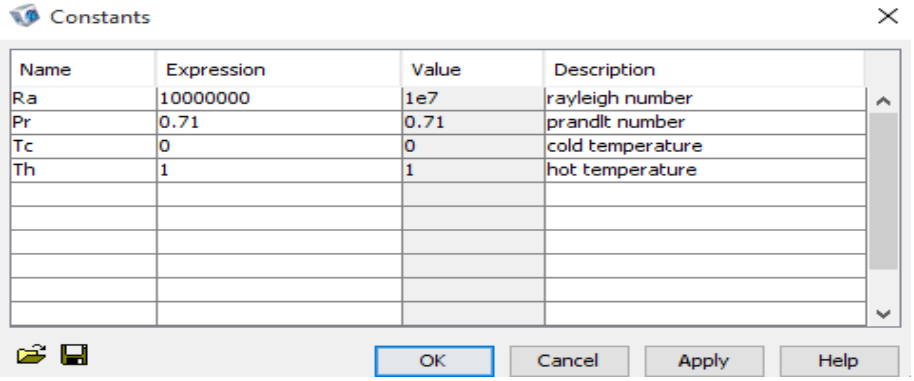

Figure 3.7: Constants table

Step 4: Physics modeling:

At this stage we enter all descriptions and settings for the physics and equations in the model for the thermal balance in each chosen application mode.

- **Subdomain Settings:** In this section we specify material properties, sources, and PDE coefficients on the subdomain that we would work with by following the subsequent instructions:

  Physics → subdomain settings → select the subdomain and then define the fluid properties (in our case it is dimensionless)

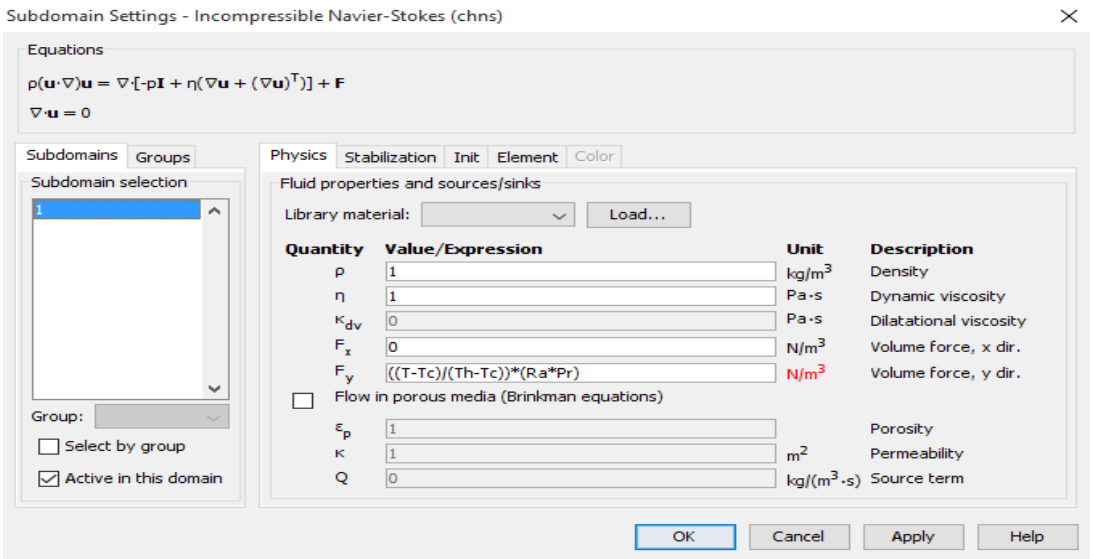

Figure 3.8: Subdomain setting window in incompressible Navier-stokes mode

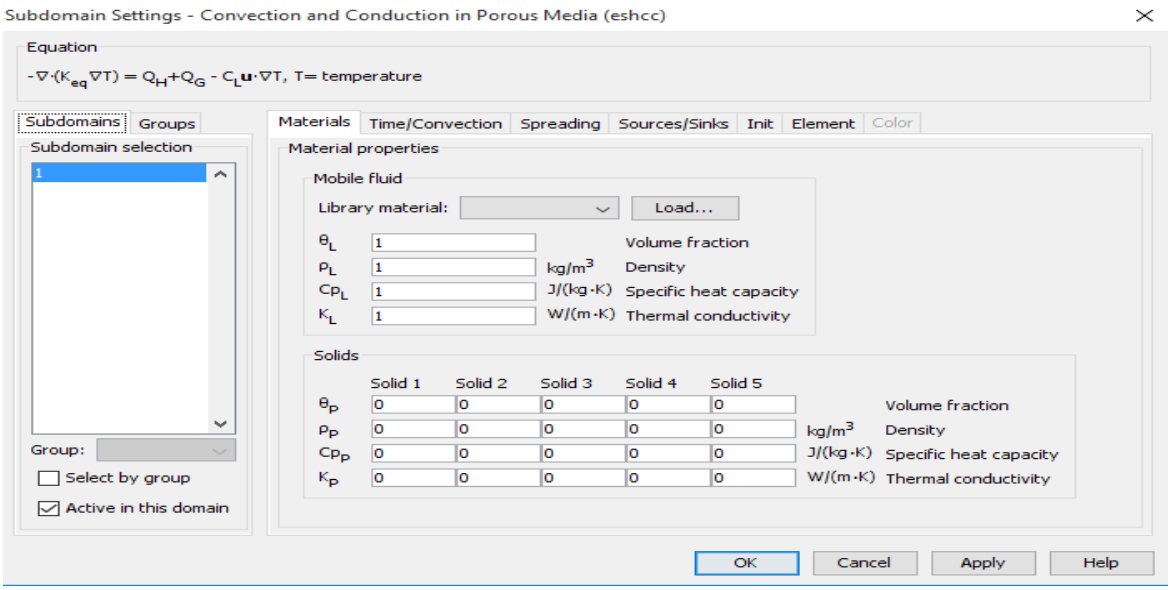

Figure 3.9: Subdomain setting window in convection and conduction in porous media mode

- **Boundary conditions:**

At this point, the boundary conditions for each border will be defined with the **Boundary setting** window, after having selected each time the border concerned and determine its specific boundary conditions then confirming.

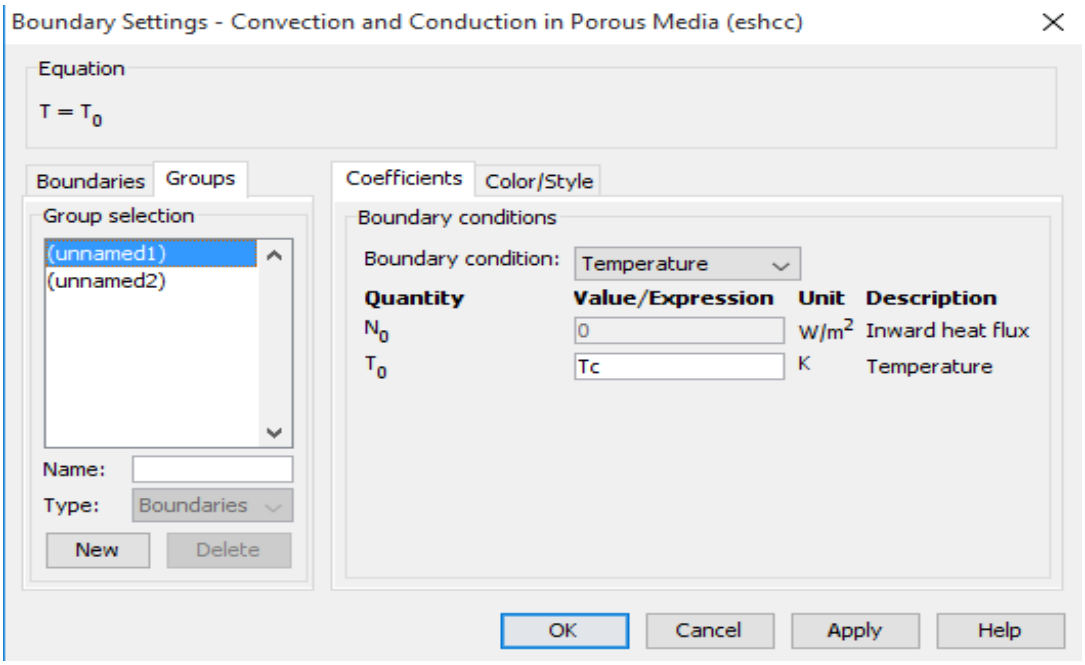

Figure 3.10: Defining the boundary condition for temperatures (T cold)

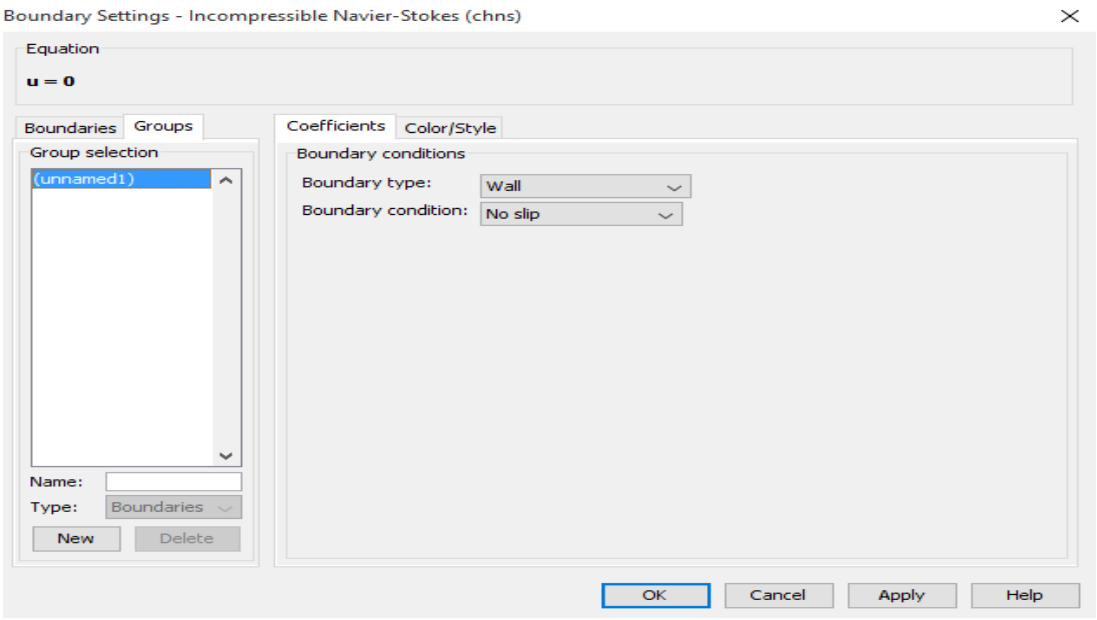

Figure 3.11: Define the boundary conditions in Incompressible Navier-stokes mode

- **Point Settings**

Here we specify point settings and describe properties and values for point source.

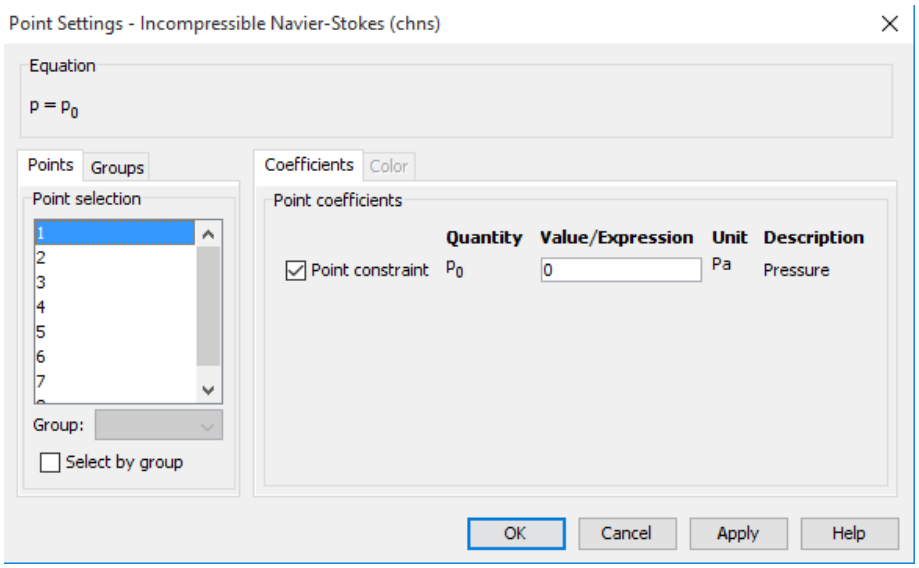

Figure 3.13: Point setting coefficients

Step 5: Mesh generation:

Once the geometry has been created, boundary conditions and subdomain physics have been defined, it is necessary to generate the finite element mesh by **initialize mesh** then **refine mesh** buttons from Main toolbar or the **Mesh** menu.

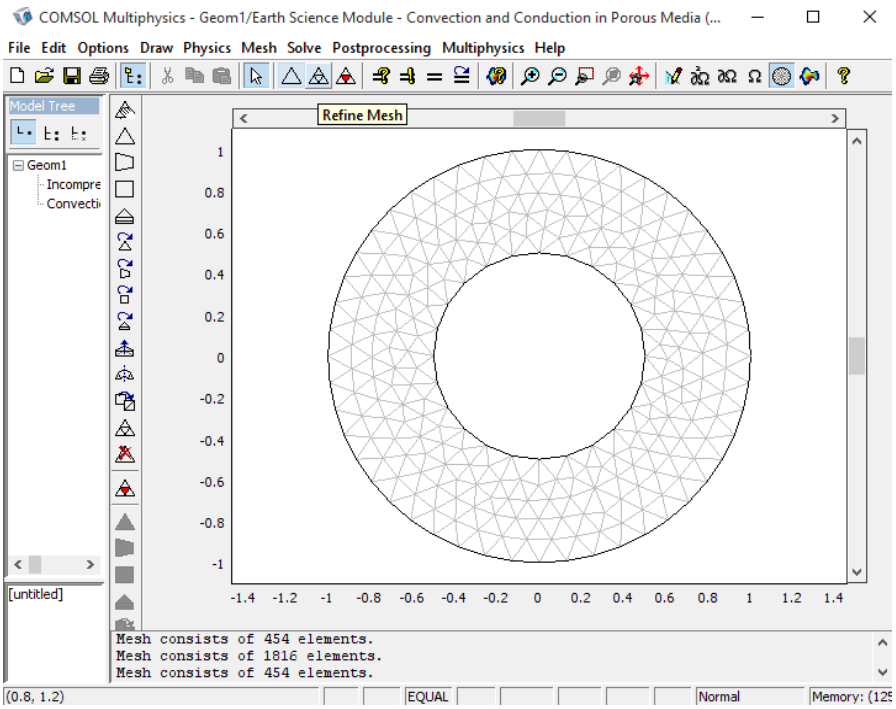

Figure 3.14: Initialized mesh

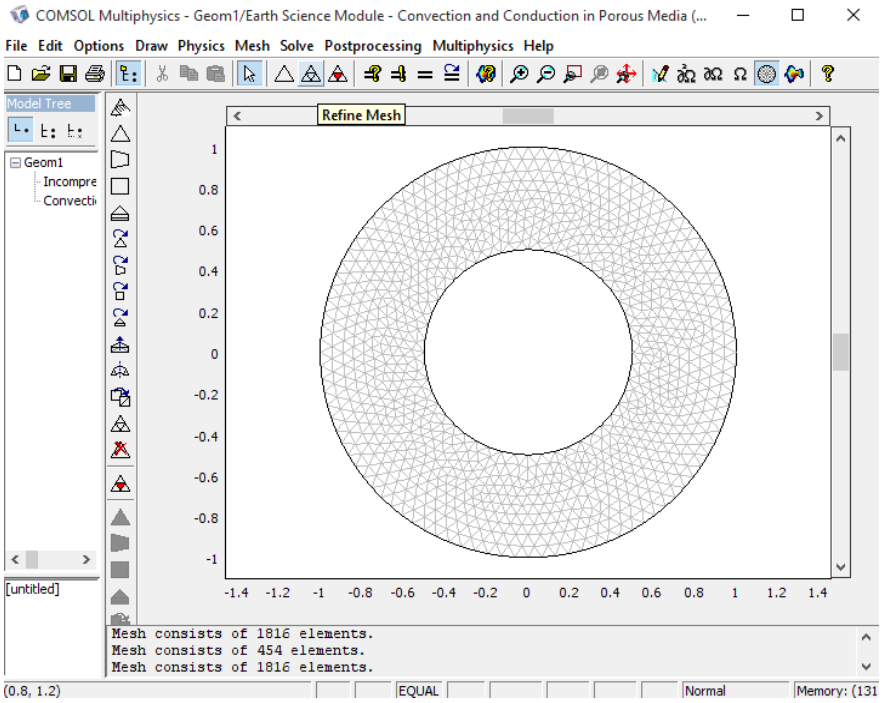

Figure 3.15: Refined mesh

Step 6: Computing the solution:

The last step before Postprocessing and results visualization is solving the model, in the **Solver Parameters** menu we have changed some solver properties as the below window show us with mentioned that the solver includes both application modes in the solution process by default.

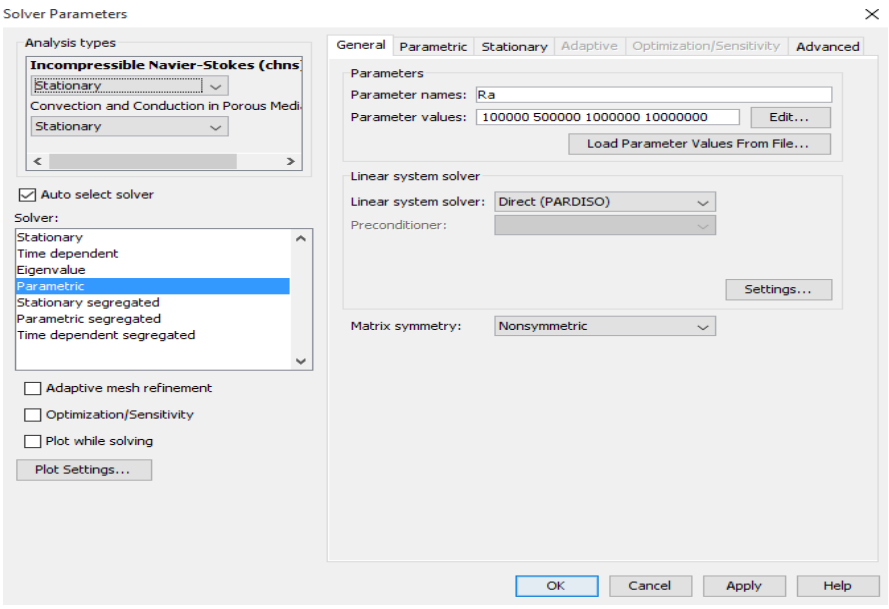

Figure 3.16: Solver parameters window

Step 7: Postprocessing and plotting

The final step is the visualization of the different results and the selection of the plot parameters.

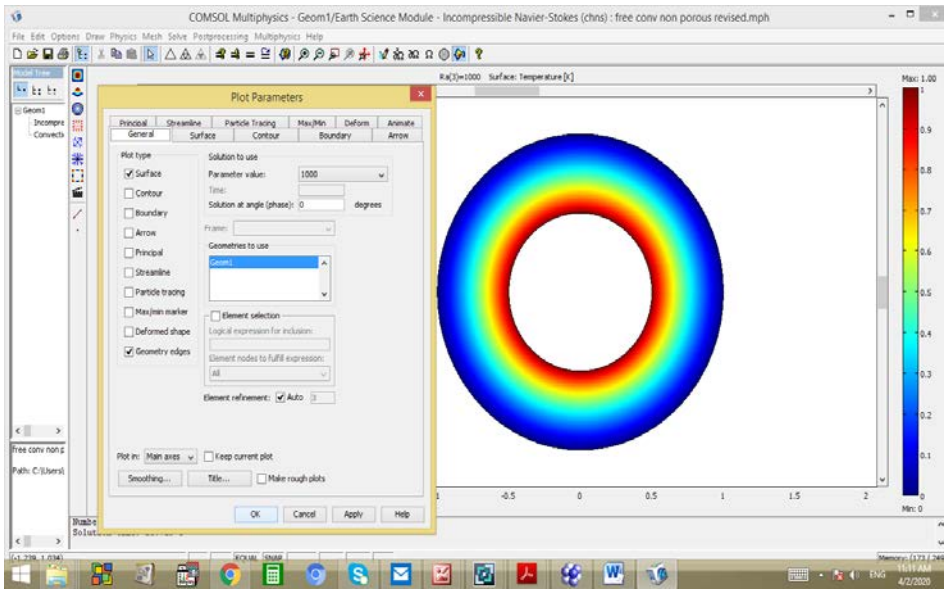

Figure 3.17: Postprocessing and results visualization

CHAPTER IV:

RESULTS AND DISCUSSION

4.1 Introduction:

In this chapter we examine in the first place our results by comparing them to similar results in literature and then we present our results in two main parts. The first part concerns the case where the physical space is filled with a Newtonian fluid and we illustrate results of the dimensionless temperature distribution and velocity field for a different Rayleigh number and aspect ratio values to examine their effects on the convective heat transfer and the flow motion within the annular cylindrical space. The fluid used is the air with Prandtl number Pr=0.71 and the Rayleigh number ranges from 10^3 to 10^7 for three values of the aspect ratio A=1.2, 2 and 3.

The second part concerns the case where the physical space is filled with fluid-saturated porous medium. We illustrate results of the dimensionless temperature distribution and velocity field in terms of Rayleigh number, the aspect ratio and permeability to examine their effects on the convective heat transfer and the flow motion. The fluid used is the air with Prandtl number Pr=0.71 and the porous medium permeability ranges from 10^{-1} to 10^{-5} m^2 and Rayleigh number ranges from 10^3 to 10^6 for three values of aspect ratio A=1.2, 2 and 3.

4.2 Numerical validation:

Upon modeling completion, the most important step to check the accuracy of the results obtained is to compare them to different literature results. To this end, the adopted model was validated and compared with three analyzes published by **[37]** Tahseen A. Al-Hattab and Dr. Majid H.Majeed, **[38]** Xiufeng Yang and Song-Charng Kong and **[39]** Fatemeh Tavakkol and Kambiz Vafai. Our simulation parameters were taken equal to those of the literature carried out in the cited works as the results were found to be in good agreement as shown in Figures (4.1), (4.2), and (4.3).

Figure (4.1) shows the contours of the temperature and velocity field of a numerical simulation described by **[37]** for Ra= $7.12x10^2$ and compared to our simulation results, it can be seen the agreement between both results. The isotherms are almost concentric circles this means that the heat transfer is dominated with conduction mode. Both results are qualitatively similar in the whole annular space for the temperature distribution which represents a conductive heat transfer, and also for the flow structure both results are showing the presence of two counter rotating cells.

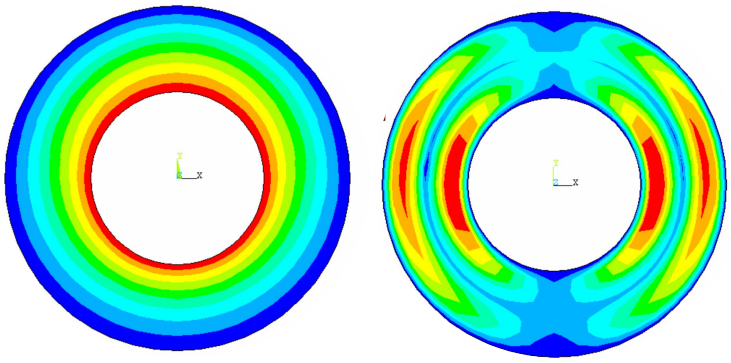

(a)

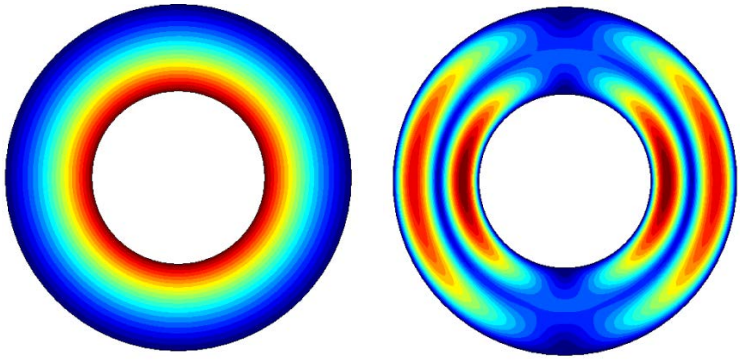

(b)

Figure 4.1: Qualitative comparison of Isotherms and streamlines for Ra= $7.12x10^2$, Pr=0.71 and A=2, (a) **[37]** and (b) the present work

Figure (4.2) shows a second comparison with the numerical resolution of **[38]** for Ra=10^4 and Pr=1. We can see that both results reproduce the same flow structure in the annular space in on hand, in the other hand the heat is not transferred with the same intensity of the convective mode base on the difference in the temperature field, especially in the upper side of the annular space.

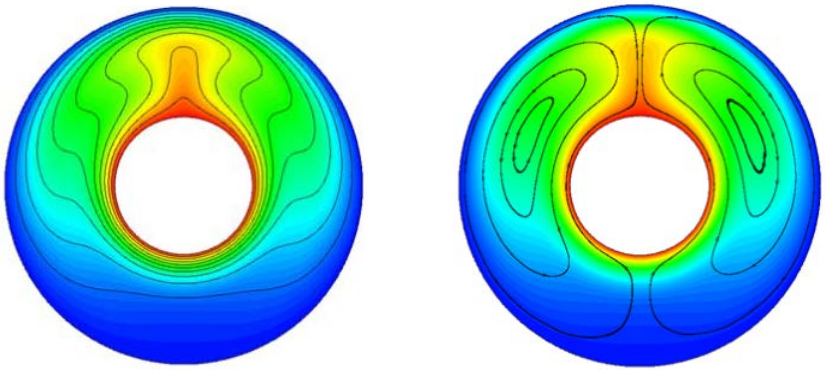

(a)

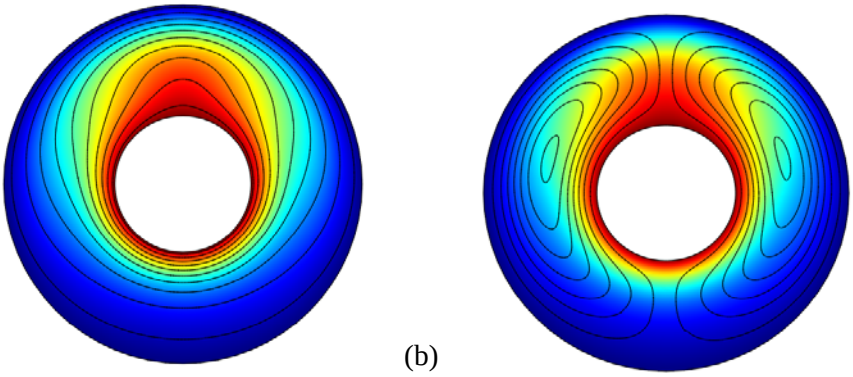

(b)

Figure 4.2: Qualitative comparison of Isotherms and streamlines for Ra=10^4, Pr=1 and A=2.6, (a) **[38]** and (b) the present work

Figure (4.3) presents a comparison between reference **[39]** and the present work. The temperature stratification is well noted as well as the convective dominance for both results. The same behavior is observed for the temperature distribution represented by of the isotherms and the flow structure represented by streamlines with a slight difference related to the intensity of the convection clearly observed.

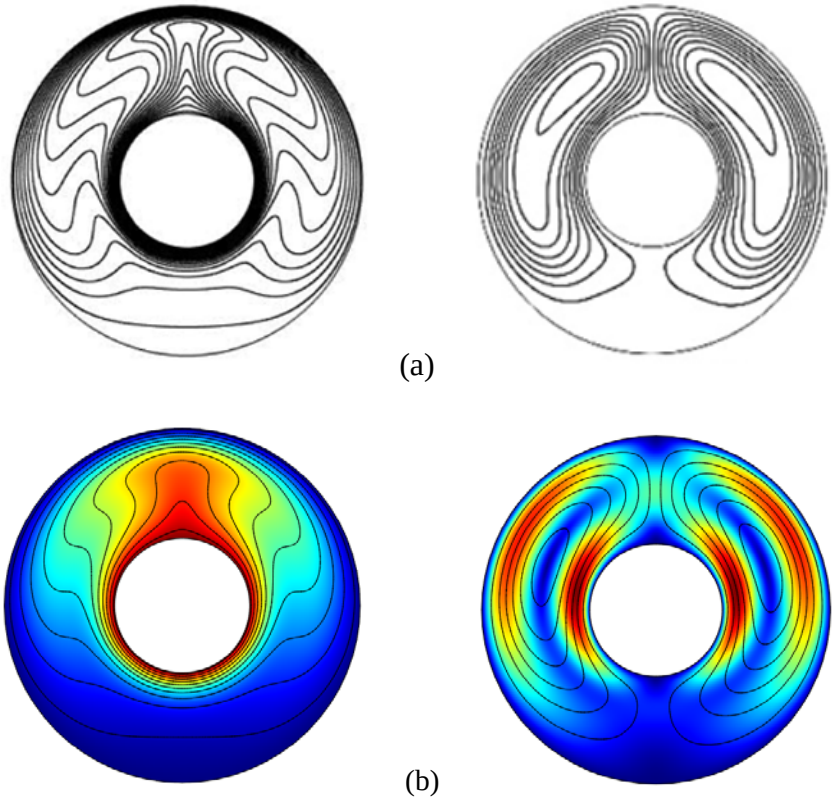

(a)

(b)

Figure 4.3: Qualitative comparison of Isotherms and streamlines for Ra=5.10^4, Pr=0.71 and A=2.6, (a) **[39]** and (b) the present work

4.3 Space filled with a fluid:

4.3.1 Effect of Rayleigh number

Figures (4.4) represents the temperature distribution (isotherms) and velocity field (streamlines) with vectors for different values of Rayleigh number ($Ra=10^3$, $Ra=10^4$, $Ra=10^5$, $Ra=10^6$ and $Ra=10^7$) where the Aspect ratio was kept constant (A=2).We can observe that these contours are symmetrical about the median fictitious vertical plane in the annular space. The isotherms in figure (4.4.a) for $Ra=10^3$are concentric closed curves which coincide with the walls profile; in this case the temperature distribution is simply decreasing from the hot wall to the cold wall. The velocity field in the same figure shows that the flow is organized in two main cells that rotate very slowly in opposite directions. This is due to the upward movement of the fluid particles which heat up along the hot wall under the buoyancy effect related to temperature gradients and the downward movements of the fluid particles which cool along the cold wall under the gravity. The fluid motion is very slow and the dimensionless velocity values are relatively low. This mode of heat transfer is dominated by a pseudo-conductive regime for the case of low Ra values. With an increase in Rayleigh value to $Ra=10^4$ isotherms deforms slightly upward announcing the presence of the convection and the dimensionless velocity is increasing but the heat transfer remains dominated by a pseudo-conductive mode accordingly to the figure (4.4.b).With a further increase in Rayleigh number as shown in Figure(4.4.c), isotherms become distorted which means that the convective mode is taking place in the upper side of the annular space and the fluid motion is dominated by a buoyancy-driven flow. In the lower space, isotherms become very close to each other near the hot wall forming a boundary layer where the pseudo conduction still acting with a slight contribution of the convection far from this boundary layer.When the increase of Rayleigh number reaches $Ra = 10^6$and $Ra=10^7$as shown in figure (4.4.d) and figure (4.4.e) respectively, we notice a net intensification of the convective mode in the whole annular space. Isotherms are completely changed from a circular concentric contours form to a wing form under the intensification of the flow motion structure which is formed by two counter rotating cells in the left and the right sides of the space. The hot fluid is gaining the upper half of the annular space, while the cold fluid is stratifying down under the buoyancy differences. The dimensionless velocity in figure (4.4.e) is increasing dramatically due to the increase of Rayleigh value especially near the walls where the fluid spinning with a high velocity while the fluid is almost motionless in the center of both convective cells.

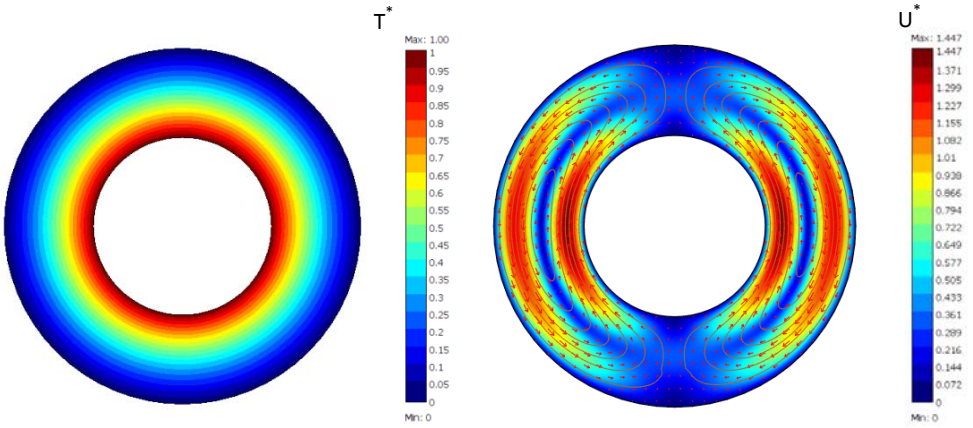

(a) Ra=10^3

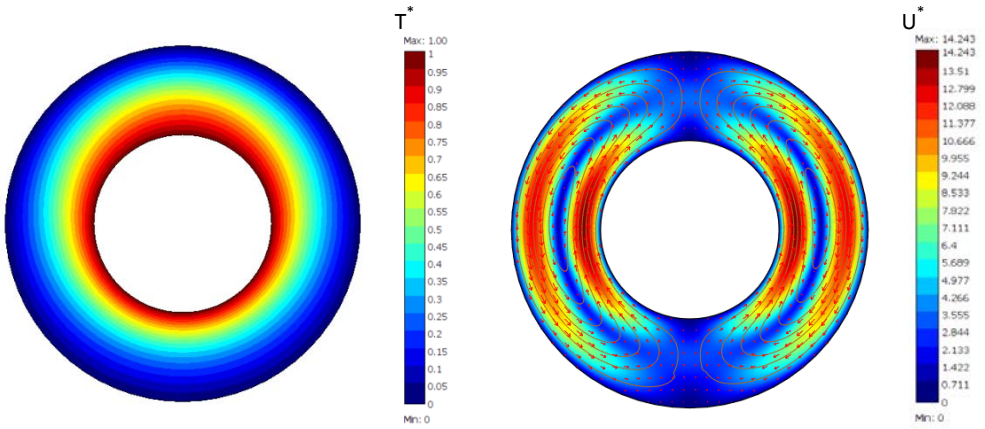

(b) Ra=10^4

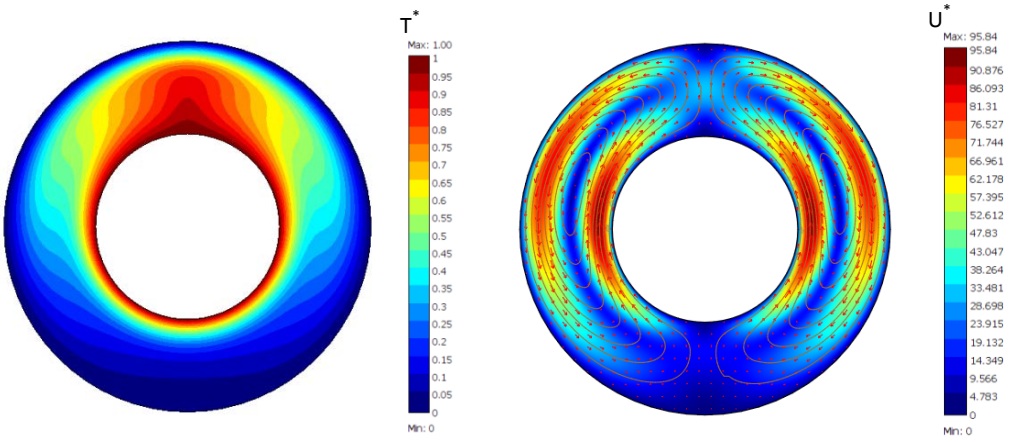

(c) Ra=10^5

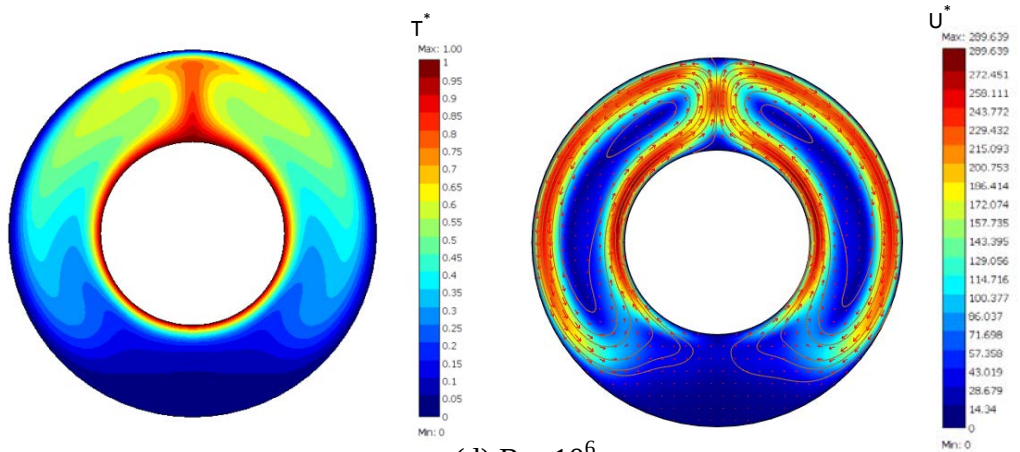

(d) Ra=10^6

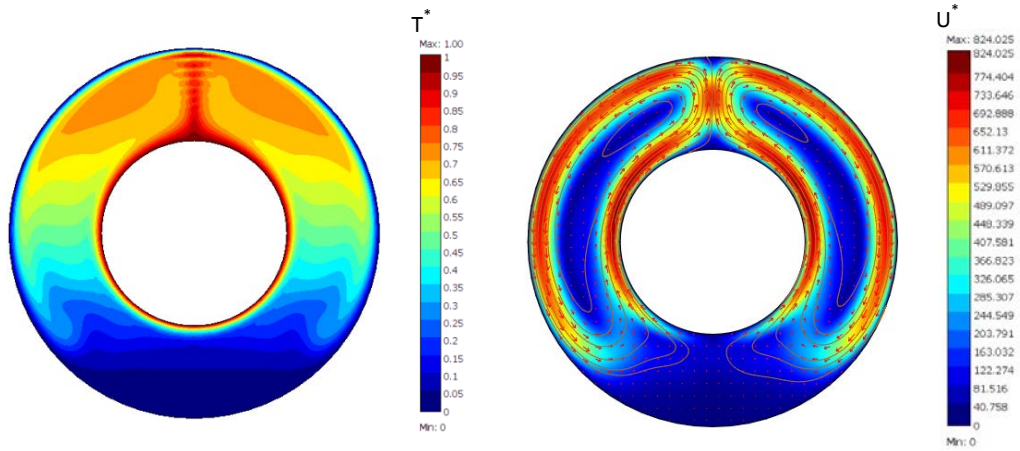

(e) Ra=10^7

Figure 4.4: Isotherms and streamlines for different values of Ra with aspect ratio A=2.

4.3.2 Effect of Aspect ratio:

Figure (4.5) represent isotherms and streamlines for the same Rayleigh number Ra=10^5 and different Aspect ratios A=1.2, A=2, A=3.

Figures illustrate that contours are symmetrical about the median fictitious vertical plane in the annular space and that the flow remains organized in two main cells that rotate in opposite directions. The isotherms in figure (4.5.a) for A=1.2 are concentric closed curves which coincide perfectly with the walls profile; in this case the temperature distribution is simply decreasing from the hot wall to the cold wall. The velocity field in the same figure shows that the flow is organized in two main cells that rotate very slowly in opposite directions. In this case, the free space between the inner and the outer cylindrical walls is very small which makes the heat transfer occurs by pseudo conduction. An increase in the value of aspect ratio will generate an increase in the air gap. This additional free space will enhance the convection as illustrated in the figure (4.5.b), where transfer by natural convection becomes more intensive especially in the upper part of the annular space under the buoyancy effect. Also

noted an increasing in the dimensionless velocity values consequently with mentioned that the maximum velocity occurs near the boundary layer of inner cylinder in both left and right sides. In the other hand, with a further increase of the free space that corresponds to A=3, isotherms in figure (4.5.c), show that heat transfer remains dominated by a convective mode and the hot air is diffused in more regions of the annular space but with a slight decrease in the intensity of the convection due to the increase in the gap.

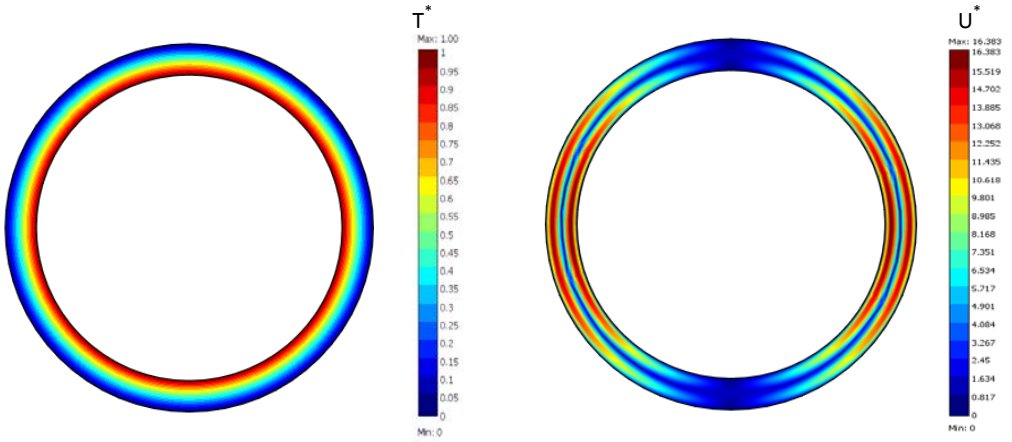

(a) A=1.2

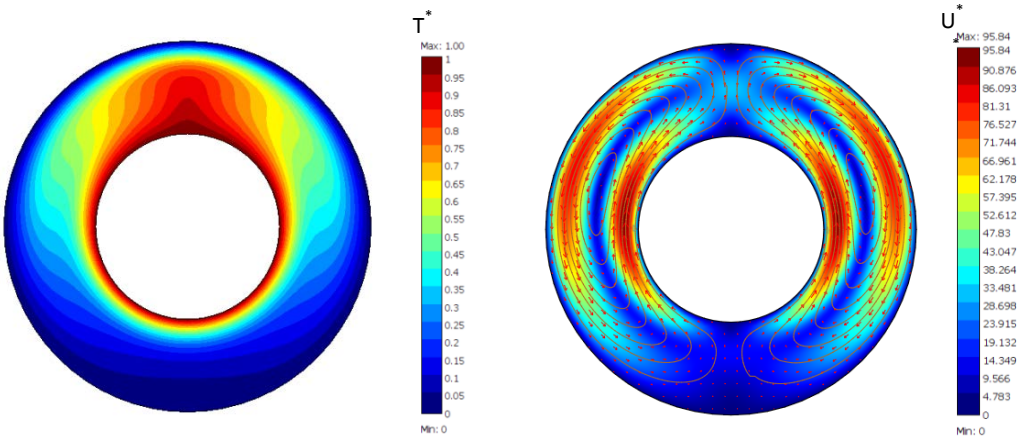

(b) A=2

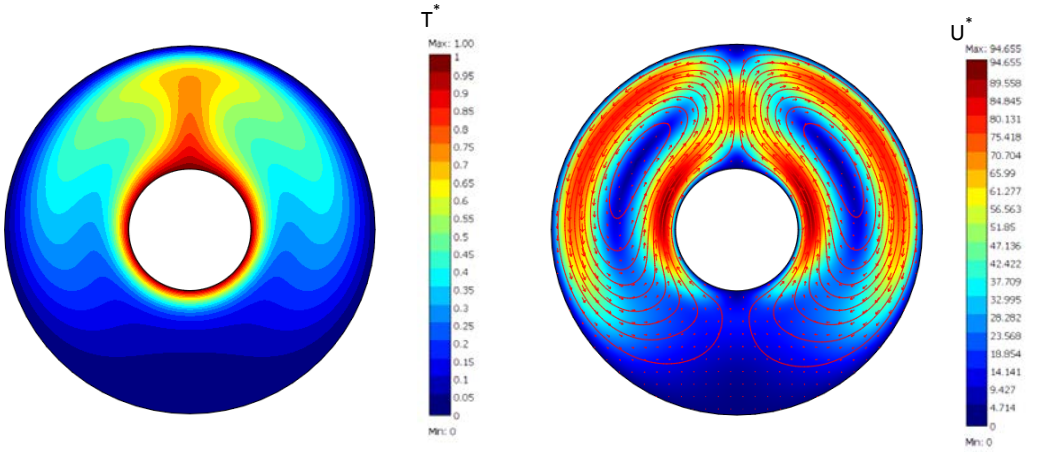

(c) A=3

Figure 4.5: Isotherms and streamlines for different values of A with Rayleigh number Ra=10^5

4.4 Space filled with a fluid-saturated porous medium:

4.4.1 Effect of Rayleigh number

Figure (4.6) represents isotherms and streamlines with vectors in order to show the flow structure and direction inside the annular space, for different Rayleigh numbers Ra=10^4, Ra=10^5 and Ra=10^6. The permeability and the aspect ratio correspond respectively to K=$10^{-3}m^2$ and A=2. Figure (4.6.a) illustrate that the isotherms are concentric closed curves for Ra=10^4 which indicates that temperature distribution is linearly decreasing from the hot wall to the cold wall. The fluid motion is very slow and the dimensionless velocity values are relatively low. This mode of heat transfer is mainly occurred by a pseudo-conductive regime. With an increase in Rayleigh number to Ra=10^5, isotherms start losing their concentric character in the upper region of the annular space, this change refers to a small contribution of the convection in the heat transfer. Other than, we note that the maximum dimensionless velocity is increased by ten time compared to velocities for Ra=10^4 in the previous figure. Even with this intensification of the convection, heat transfer is still dominated by a pseudo-conductive mode especially in the lower region of the space as illustrated in the figure (4.6.b). Once Rayleigh number is raised up to Ra=10^6 as shown in figure (4.6.c), isotherms become deformed which means that the natural convection is fully developed in the upper region of the annular space. In the other hand, isotherms form a boundary layer in the lower region near the inner cylinder where the conduction is the main mode for heat transfer within this thermal layer and under this intensification of the convective mode, velocities are increased drastically.

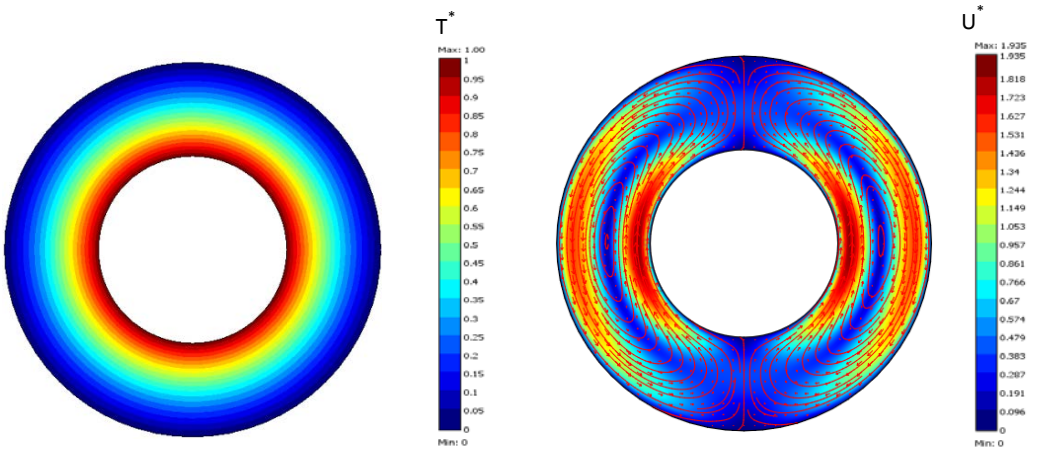

(a) Ra=10^4

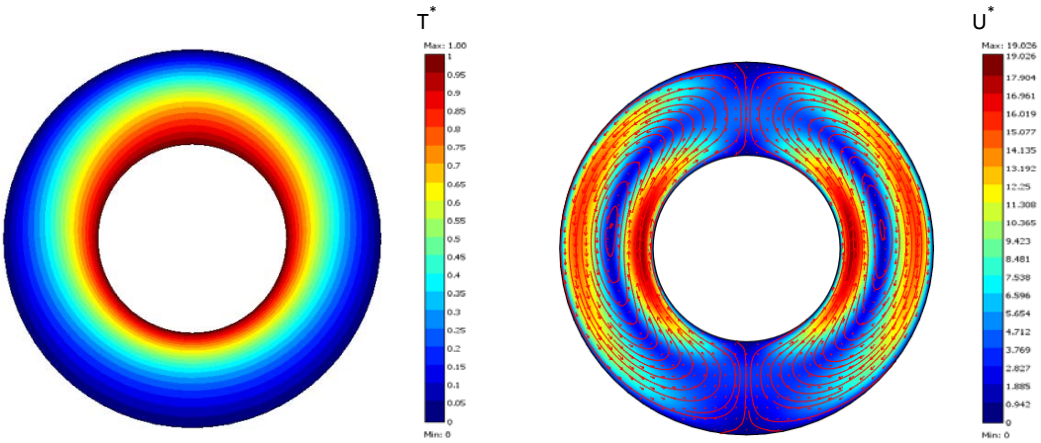

(b) Ra=10^5

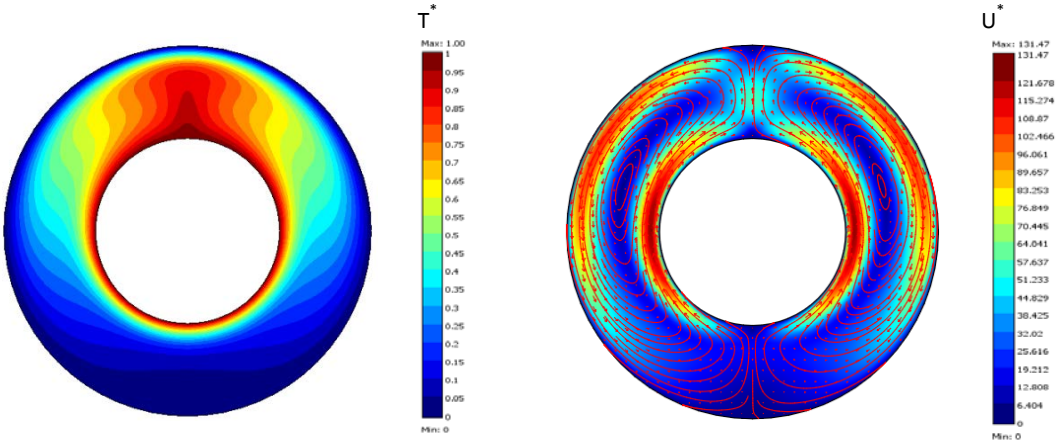

(c) Ra=10^6

Figure 4.6: Isotherms and streamlines for different values of Rayleigh number Ra with aspect ratio A=2 and permeability K=$10^{-3}m^2$

4.4.2 Effect of Permeability

Figure (4.7) represents isotherms and streamlines for different permeability values from $K=10^{-1}\ m^2$ to $K=10^{-4}\ m^2$ for a determined aspect ratio A=2 and Rayleigh number $Ra=10^5$. We can observe that these contours are symmetrical about the median fictitious vertical plane and the flow is organized in two main cells that rotate in opposite directions. In figure (4.7.a) for $K=10^{-1}\ m^2$ which is considered high permeability, The isotherms are rising upward which means that heat transfer is dominated by a convective mode in the upper region in contrary to the lower region that still under a pseudo conduction. The velocity field in the same figure shows that the fluid motion is relatively important. The fluid is pushed towards the inner and the outer walls through the porous medium and the convective cells are adjacent in the upper and the lower regions of the annular space. With a decrease in the permeability to $K=10^{-2}\ m^2$ the figure (4.7.b) exhibits that isotherms are slightly affected by this change as well as a decrease in the dimensionless velocity values but the flow structure is almost the same and the heat transfer remains dominated by the convective mode. With a further decrease in porous medium permeability to $K=10^{-3}\ m^2$, figure (4.7.c) illustrate that isotherms are recessed to an eccentric closed curves configuration under the diminution of the porous channels which affected the flow by an evident decreasing in the dimensionless velocity values and the pseudo-conductive heat transfer regime becomes preponderant with a slight contribution of the convection regime.

Figure (4.7.d) shows that with a furthermore decrease in the permeability to $K=10^{-4}\ m^2$, the low permeability affectes the flow behavior and begin gradually resisting the flow motion until the isotherms become clearly a concentric circles and the pseudo-conduction completely dominates the heat transfer regime in the whole annular space. The velocity field in the same figure exhibits a net decrease in the dimensionless velocity values with the permeability decrease; we can note that flow rotating cells are splaying away in opposite directions leaving a gap in both upper and lower regions due to dominance of the pseudo-conduction in the whole space, this regime is known as creeping flow where the fluid motion is slowed down by the porous medium that is characterized by low permeability.

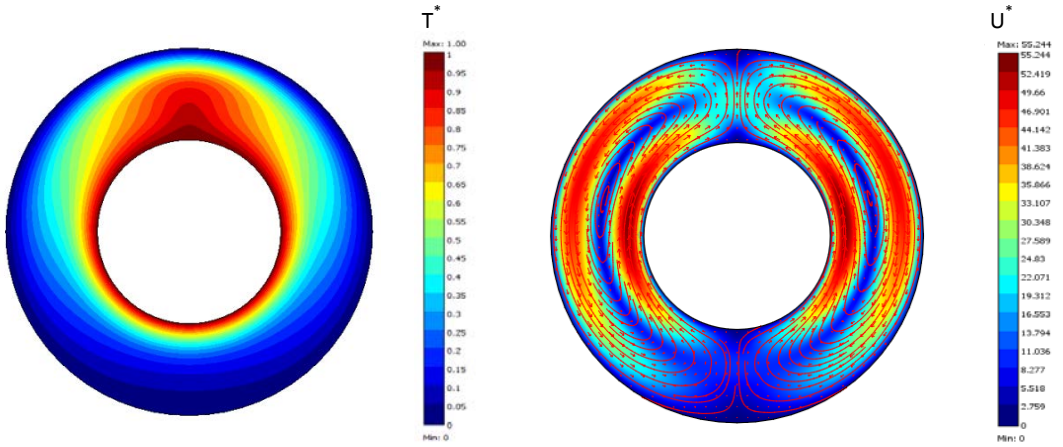

(a) $K=10^{-1}m^2$

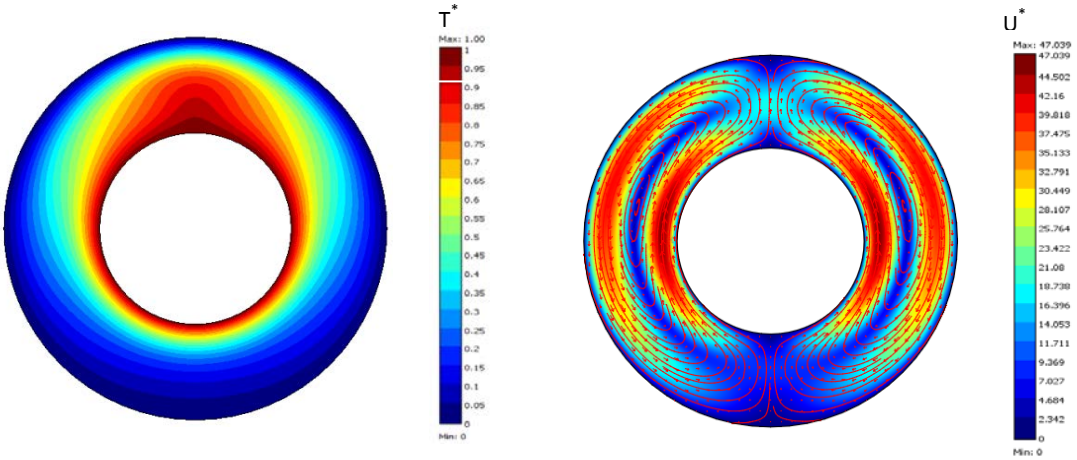

(b) $K=10^{-2}m^2$

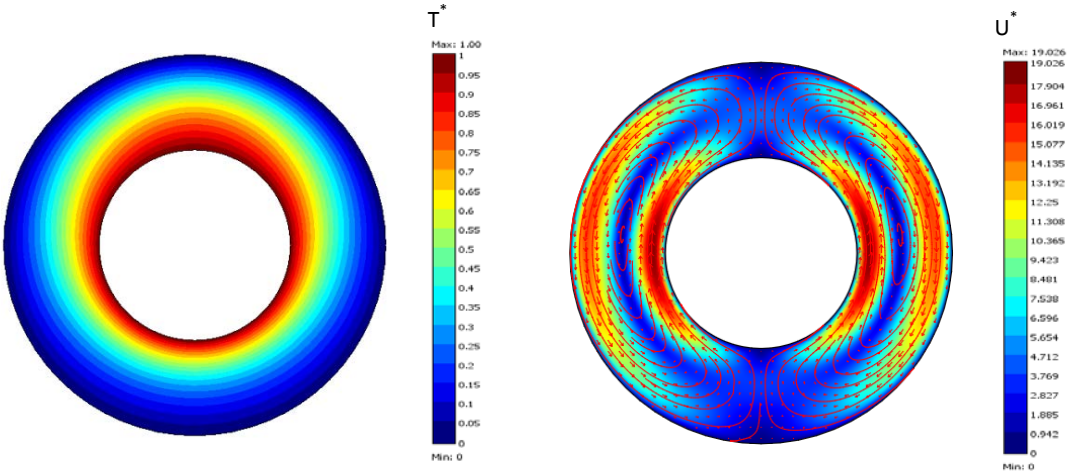

(c) $K=10^{-3}m^2$

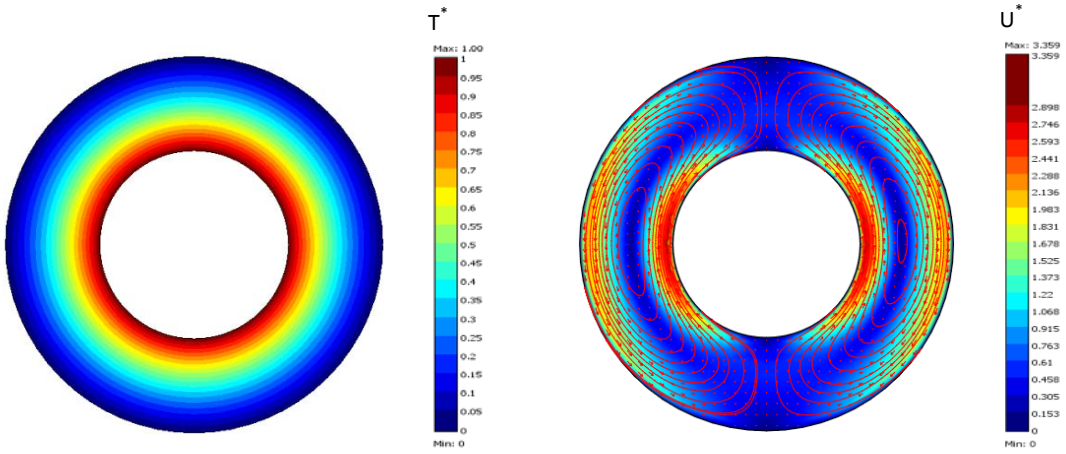

(d) $K=10^{-4}m^2$

Figure 4.7: Isotherms and streamlines for different values of permeability K with Rayleigh number $Ra=10^5$ and aspect ratio A=2

4.4.3 Effect of aspect ratio

Figure (4.8) represents isotherms and streamlines for the same Rayleigh number $Ra = 10^5$ and the same permeability $K=10^{-3}m^2$ but for different aspect ratios A = 1.2, A = 2, A = 3.

as it shown in figure (4.8.a) when A = 1.2, The air gap between the inner and outer cylindrical walls is very small and tight which doesn't allow the fluid to circulate freely in this region which means that the convection will not have enough space to develop and as a result, the temperature distribution is simply decreased from the hot wall to the cold wall and isotherms are concentric closed curves that perfectly match the walls profiles. The velocity field shows that the flow is organized in two main cells that rotate very slowly in opposite directions. The heat transfer is dominated by pseudo-conduction regime. When we create more free space in figure (4.8.b) by raising the value of aspect ratio to A=2 the gap is increased consequently, isotherms shows a slight deflection upwards refer to a small contribution of the convection, the dimensionless velocity increases but heat transfer still dominated by pseudo-conduction. With a further increase in aspect ratio to A=3 the free space will have an additional expansion that have boosts the convective flow to become more intensive in the upper part of the annular space and that what we noted in figure (4.8.c) where isotherms became distorted under the intensification of the natural convection and we can clearly observe a net increase in the dimensionless velocity as well.

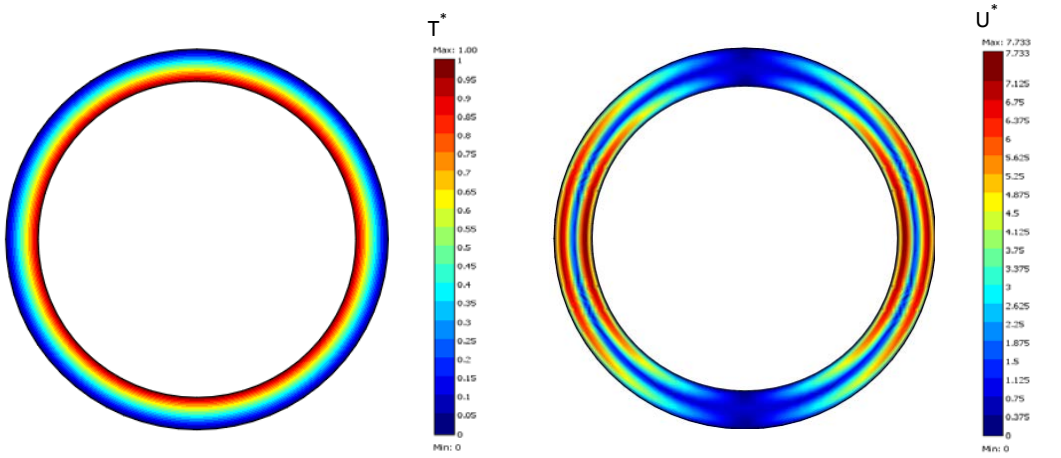

(a) A=1.2

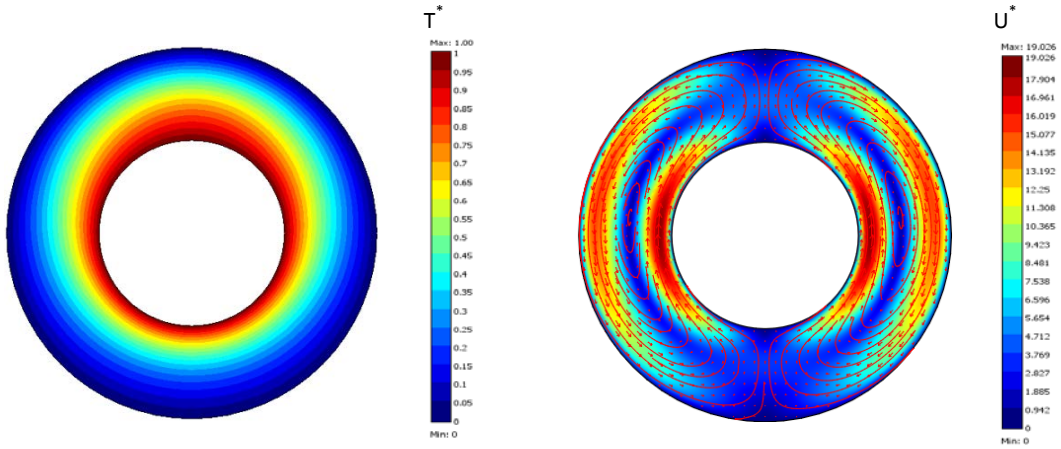

(b) A=2

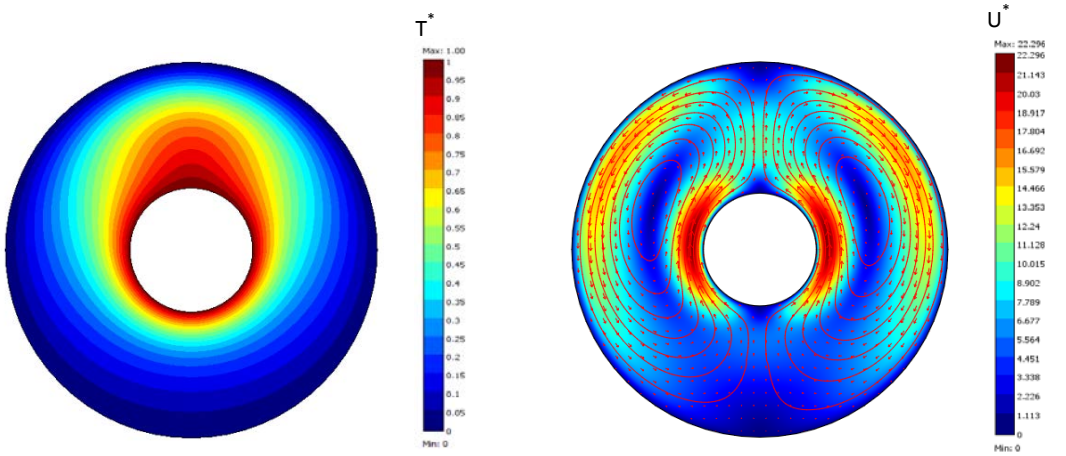

(c) A=3

Figure 4.8: Isotherms and streamlines for different values of aspect ratio A with Rayleigh number $Ra=10^5$ and permeability $K=10^{-3}m^2$.

Conclusion

In the present study we presented a two-dimensional numerical simulation in a cylindrical heat pipe cross section that was successfully made using Comsol Multiphysics software. A single phase steady state approach was used to achieve the computation of a laminar natural convection in the horizontal annular space which is filled with a Newtonian fluid in the first case and with a fluid saturated porous medium in the second one. Governing equation are the Navier stocks equations and energy equation with the assumption of Boussinesq. With regard the porous medium constitutive model, we have selected a Brinkman's model which is considered as an extension of the Darcy's model.

As a first objective, we studied the influence of specific parameters including Rayleigh number; aspect ratio and permeability on the fluid flow and on heat transfer. The dimensionless temperature distributions and velocity field were plotted according to these different control parameters. The numerical results were found to be in very good agreement with those in the literatures from a qualitative point of view.

We examined the effect of Rayleigh number that considerably influenced the nature and the structure of the flow; the results have shown in both cases that for low Rayleigh number heat transfer is dominated by the pseudo-conduction regime in the whole annular space. But with the increase in its value, the flow becomes more pronounced so the convective regime appears and dominates the heat transfer within the space with an important intensity in the upper part of the annular space particularly.

Furthermore the influence of the geometry on the thermal natural convection was also examined in both cases for different aspect ratio, we summarized that heat transfer is improved when the free space between the two cylinders increases what made natural convection have enough space to develop and present further intensification with each additional expansion in the annular space. Other than, at the small tight free spaces the fluid cannot freely circulate what makes its motion insignificantly and heat transfer is only occurred by pseudo conduction mode.

The permeability effect is also investigated in the second case. On one hand, we have observed that the fluid flow is more significant for high permeability which led to high velocity gradients and allows the convection to intensify in the upper part of the horizontal annular space. On the other hand, low permeability inhibited the flow inside the annular

enclosure and led to a relatively slow fluid motion. In this case heat transfer is completely dominated by the pseudo conductive regime due to the high flow resistance.

Finally, as our study focused on a simplified example of a particular geometry and the simulation focused on the problem of natural convection, it would be interesting in the future to consider other more phenomenon that occurs inside a heat pipe as evaporation and condensation, we can also consider the turbulent flow and capillarity forces which are available in the data base of Comsol Multiphysics.

References

[1] J.P. Holman, Heat transfer, 10th ed, Mcgraw-Hill Series In Mechanical Engineering, (2010)

[2] John L. Monteith and Mike H. Unsworth, Principles of environmental physics, 4th ed, pp.151-178, (2013)

[3] https://www.tes.com/lessons/h4H_AYNgmFhlEA/copy-of-heat-transfers

[4] Bahman Zohuri, Heat Pipe Design and Technology: Modern Applications for Practical Thermal Management, University of New Mexico.USA, (pp.1-41), (2016).

[5] http://celsiainc.com/heat-sink-blog/heat-pipes-vapor-chambers-difference/

[6] Y. Lee and A. Bedrossian, The Characteristics of Heat Exchangers using Heat Pipes or Thermosyphon, Int. J. of Heat and Mass Transfer, Vol.21, pp. 221-229, (1978)

[7] Ma, H. B et al., Effect of nanofluid on the heat transport capability in an oscillating heat pipe, Applied Physics Letters, Vol.88, pp.143116-143119, (2006)

[8] C. Y. Tsai et al., Effect of structural character of gold nanoparticles in nanofluid on heat pipe thermal performance, material letters, Vol.58, pp.1461-1465, (2004)

[9] K. Fang, C. Weng, S. Ju, An investigation into the structural features and thermal conductivity of silicon nanoparticles using molecular dynamics simulations, Nanotechnology, Vol.17, pp. 3909-3914, (2006)

[10] https://en.wikipedia.org/wiki/Heat_pipe

[11] X. Chen et al., A review of small heat pipes for electronics, applied thermal engineering, Vol.96, pp.1-17, (2015)

[12] X. Yang, Y. Yan and D. Mullen, Recent developments of lightweight, high performance heat pipes, Applied thermal engineering, Vols.33-34, pp.1-14, (2012)

[13] S. Riffat and X. Zhao, A novel hybrid heat pipe solar collector/CHP system—Part 1: System design and construction, Renewable energy, Vol. 29, pp.2217-2233, (2004)

[14] S. Riffat, X. Zhao, R. Boukhanouf and P. Doherty, Theoretical and experimental investigation of a novel hybrid heat-pipe solar collector, International journal of green energy, Vol.1, pp.515-542, (2005)

[15] V.H. Gray, The rotating heat pipe-A wickless, hollow shaft for transferring high heat fluxes, ASME PAPER 69-HT-19 (1969)

[16] L. Zhu et al., Investigation of heat pipe cooling in drilling applications: Part 2-Thermal, structural static and dynamic analyses, American Society of Mechanical Engineers, pp. 2027-2034, (2009)

[17] Daniel J. Kearney, Omar Suleman and Justin Griffin, an experimental analysis of an open loop pulsating heat pipe operating with a dielectric working fluid for embedded power electronic applications, IHTC15-9656, August 10-15, 2014, Kyoto, Japan.

[18] Xiangdong Liu and Yongping Chen, Transient thermal performance analysis of micro heat pipes, Applied Thermal Engineering, Volume 58, Issues 1–2, September 2013, pp. 585-593

[19] CHEN X., YE H., FAN X., et al., A review of small heat pipes for electronics, Applied thermal Engineering - vol. 96, pp. 1-17 (2016).

[20] https://www.1-act.com/innovations/heat-pipe-materials-working-fluids-and-compatibility/

[21] https://www.1-act.com/innovations/heat-pipes/

[22] https://cooltechnologiesinc.com/thermal-dispersion/heat-pipes/

[23] Eui Guk Jung and Joon Hong Boo, A Novel analytical modeling of a loop heat pipe employing the thin-film theory: Part I—modeling a simulation, Vol.12, (2019).

[24] E. Mezaache. A. OmaraandM.S. Ferah, Etude numérique et expérimentale d'un caloduc a conductance variable (CCV), science &Technologie-N°12, pp.25-32, (1999)

[25] K.H. Sun and C.L. Tien, Thermal performance characteristic of heat pipe, Int.J. Heat Mass Transfer, Vol.18, pp. 363-380, (1975)

[26] Boulahrouz Salim, Etude de la performance d'un thermosiphon diphasique utilise pour le refroidissement de composants électroniques de puissance, Thèse de doctorat, Université Badji Mokhtar – Annaba, (2008)

[27] Hamidreza Behi, Experimental and Numerical Study on heat pipe assisted PCM storage system, Master of Science Thesis, KTH School of Industrial Engineering and Management, (2015)

[28] Vikas Kumard, Gangacharyulu and Ram Gopal Tathgir, Heat transfer studies of a heat pipe, Heat Transfer Engineering, Vol.28, pp.954-965, (2007)

[29] Nicolas Blet, Stéphane Lips and Valérie Sartre, Heats pipes for temperature homogenization: A literature review, Applied Thermal Engineering ,Vol.118, Pages 490-509, (2017)

[30] Cheayb Mohamad, Modélisation des comportements hydrodynamiques et thermiques d'un caloduc plat pourvue des ailettes, Mémoire de master, Université de Caen Normandie, Saint Lo. France, (2015)

[31] Lora Kamenova, Modélisation thermo-hydraulique de caloducs miniatures plats à faible épaisseur pour des applications électroniques, Thèse de doctorat, L'INP Grenoble et de l'université technique de Sofia, (2007)

[32] Mehdi Famouri, Numerical analysis of phase change, Heat transfer and fluid Flow within Miniature Heat Pipes, Doctoral dissertation, University of South Carolina, (2017)

[33] Mohamed noorul hussain and Isam janajreh, Numerical Simulation of a Cylindrical Heat Pipe and Performance Study, Int. J. of Thermal & Environmental Engineering Vol.12, pp.135-141, (2016)

[34] https://www.aerodefensetech.com/component/content/article/adt/features/-articles/25244

[35] H. Beji, D. Gobin, Influence of thermal dispersion on natural convection heat transfer in porous media, Vol.22, pp.487-500, (1992)

[36] Comsol Multiphysics quick start and quick reference book version 3.5a © copyright 1998–2008

[37] Tahseen A. Al-Hattab, Majid H. Majeed and Mushtaq F. Abd-Saada, Heat transfer by free convection between horizontal concentric pipes, The Iraqi Journal for Mechanical and Material Engineering, Vol.8, No.3 , (2008)

[38] Xiufeng Yang, Song-Charng Kong, Numerical study of natural convection states in a horizontal concentric cylindrical annulus using SPH method, Engineering Analysis with Boundary Elements 102, pp.11–20 (2019)

[39] Xing Yuan, Fatemeh Tavakkol and Kambiz Vafai, Analysis of Natural Convection in Horizontal Concentric Annuli of Varying Inner Shape, Numerical Heat Transfer, Part A, V.68, pp. 1155–1174, (2015)

Abstract

The presented work is a two-dimensional simulation of heat transfer by a laminar natural convection in a cylindrical heat pipe. The annular space has been categorized into two cases, in the first case; the space is filled with a fluid and in the second is filled with a fluid-saturated porous medium. The model was described by continuity, momentum and energy equations in the cylindrical coordinates system using Boussinesq's approximation and Brinkman's equation. The simulation was obtained with Comsol Multiphysics software and the effects of Rayleigh number, aspect ratio and permeability on the temperature and the velocity fields were studied. The results obtained were validated and found to be relatively in a good agreement with those in the literatures.

Keywords: Natural convection, heat pipe, porous medium, Brinkman's equation.

ملخص

العمل المقدم هو محاكاة عددية ثنائية الأبعاد للتحويل الحراري عن طريق الحمل الحراري الصفحي في أنبوب حراري أسطواني الشكل. تم تصنيف الفراغ الحلقي إلى حالتين ، في الحالة الأولى يمتلئ الفراغ بسائل، وفي الثانية يمتلئ بوسط مسامي مشبع بسائل. تم وصف النموذج بواسطة معادلات الاستمرارية و كمية الحركة والطاقة في نظام إحداثيات أسطواني باستخدام تقريب بوسينسك ومعادلة برينكمان و أجريت المحاكاة باستخدام برنامج Comsol Multiphysics. دراسة شملت تأثير عدد رايلي ومعامل الشكل ونفاذية الوسط المسامي على توزيع الحرارة ومجالات السرعة داخل الفراغ الحلقي تحت تأثير الحمل الحراري الطبيعي. تم التحقق من صحة النتائج ووجدت متوافقة نسبيا مع تلك الموجودة في الأعمال المشابهة من مراجع مختلفة.

كلمات مفتاحية : الحمل الحراري الطبيعي ، أنبوب حراري ، وسط مسامي ، معادلة برينكمان.

Résumé

Le travail présenté est une simulation bidimensionnelle du transfert de chaleur par convection naturelle laminaire dans un caloduc cylindrique. L'espace annulaire a été classé en deux cas, dans le premier cas; l'espace est rempli d'un fluide et dans le second est rempli d'un milieu poreux saturé de fluide. Le modèle a été décrit par des équations de continuité, de quantité de mouvement et d'énergie dans le système de coordonnées cylindriques en utilisant l'approximation de Boussinesq et l'équation de Brinkman. La simulation a été obtenue à l'aide du logiciel Comsol Multiphysics. Les effets du nombre de Rayleigh, du rapport d'aspect et de la perméabilité sur les champs de températures et de vitesses ont été étudiés. Les résultats obtenus ont été validés montrant un accord relativement bon avec ceux de la littérature.

Mots clés: Convection naturelle, caloduc, milieu poreux, l'équation de Brinkman.